

FINAL REPORT FOR  
NASA GRANT NCC 2-492

DEC 23 1993

*Final -  
11-25-93  
198592  
83 p*

APPLICATION AND DEVELOPMENT  
OF THE  
SCHWINGER MULTICHANNEL SCATTERING  
THEORY AND THE  
PARTIAL DIFFERENTIAL EQUATION THEORY  
OF ELECTRON-MOLECULE SCATTERING

by

Charles A. Weatherford  
Professor and Chairman  
Department of Physics  
Florida A&M University  
Tallahassee, FL 32307

Telephone: (904)-599-3470  
(904)-599-3642  
Telefax: (904)-599-3577  
E-Mail: weatherford@scri.fsu.edu

December 17, 1993

(NASA-CR-194774) APPLICATION AND  
DEVELOPMENT OF THE SCHWINGER  
MULTICHANNEL SCATTERING THEORY AND  
THE PARTIAL DIFFERENTIAL EQUATION  
THEORY OF ELECTRON-MOLECULE  
SCATTERING Final Report (Florida  
Agricultural and Mechanical Univ.)  
83 p

N94-24798

Unclass

G3/72 0198582

This is the final report for NASA grant NCC 2-492 entitled "Application and Development of the Schwinger Multichannel Scattering Theory and the Partial Differential Equation Theory of Electron-Molecule Scattering." It consists of three unpublished papers as follows:

1. "Variation of the projection parameter in a Schwinger multichannel method" by Winifred M. Huo and C.A. Weatherford;
2. "Schrödinger Equation Mesh Requirements in the Finite Difference Discretization for Non-Spherical Potentials", by Charles A. Weatherford;
3. "Completion of hybrid theory calculation of the  $\Pi_g$  resonance in electron- $N_2$  scattering", by C.A. Weatherford and A. Temkin.

Paper number three is currently under review by the Physical Review A. Paper two will shortly be submitted for publication. Paper number one will be resubmitted after further work is done.

Variation of the projection parameter in a Schwinger multichannel method

Winifred M. Huo

NASA Ames Research Center, Mail Stop 230-3, Moffett Field, California 94035

and

C. A. Weatherford

Department of Physics and Institute of Molecular Computations

Florida A & M University, Tallahassee, Florida, 32307

PACS 34.80.Bm, 34.80.Dp, 34.80.Gs

This paper was prepared for submittal to Physical Review A1

## Abstract

One version of the multichannel theory for electron-target scattering based on the Schwinger variational principle, the SMC method, requires the introduction of a projection parameter (K. Takatsuka and V. McKoy, Phys. Rev., A24, 2473 (1981)). The role of the projection parameter  $a$  is investigated and it is shown that the principal-value operator in the SMC equation is Hermitian regardless of the value of  $a$  as long as it is real and nonzero. In a basis that is properly orthonormalizable, the matrix representation of this operator is also Hermitian. The use of such basis is consistent with the Schwinger variational principle because the Lippmann-Schwinger equation automatically builds in the correct boundary conditions. Otherwise, an auxiliary condition needs to be introduced, and Takatsuka and McKoy's original value of  $a$  is one of the three possible ways to achieve Hermiticity. In all cases but one,  $a$  can be uncoupled from the Hermiticity condition and becomes a free parameter. An equation for  $a$  based on the variational stability of the scattering amplitude is derived; its solution has an interesting property that the scattering amplitude from a converged SMC calculation is independent of the choice of  $a$  even though the SMC operator itself is  $a$ -dependent. This property provides a sensitive test of the convergence of the calculation. For a static-exchange calculation, the convergence requirement only depends on the completeness of the one-electron basis, but for a general multichannel case, the  $a$ -invariance in the scattering amplitude requires both the one-electron basis and the  $N+1$ -electron basis to be complete. The role of  $a$  in the SMC equation and the convergence property are illustrated using two examples: e-CO elastic scattering in the static-exchange approximation, and a two-state treatment of the e-H<sub>2</sub>  $X^1\Sigma_g^+ \rightarrow b^3\Sigma_u^+$  excitation.

## I. Introduction

Most of the recent progress in electron-atom and electron-molecule collisions are based on variational principles. The Kohn<sup>1-4</sup> (particularly the S-matrix Kohn<sup>5,6</sup>) variational principle, the variational R-matrix method,<sup>4,7</sup> and the Schwinger variational principle<sup>8-10</sup> have all met with considerable success. Among the methods based on the Schwinger variational principle, the multichannel formulation of Takatsuka and McKoy,<sup>11,12</sup> sometimes referred to as the SMC method, is unique in the sense that its dynamical equation is derived from a combination of Lippmann-Schwinger and Schrödinger equations. In this method, the partitioning of open and closed channel space is achieved by a projection operator which operates on the target electrons alone. The open channel contribution is described by a projected Lippmann-Schwinger equation and the closed channel contribution by the Schrödinger equation. Takatsuka and McKoy introduced a parameter ' $a$ ' to the projection operator. They argued that the choice of  $a$  is uniquely determined by the requirement that the principal-value operator in their equation, represented in a basis which includes non  $\delta$ -function orthonormalizable continuum functions, must be Hermitian. Numerical calculations<sup>13-26</sup> based on this choice of  $a$  are generally in good agreement with experiment and with calculations using other methods.

Recently we initiated a study of the parameter  $a$ , which we call the 'projection parameter', in the SMC method. We begin with the premise that an optimal choice of  $a$  should provide a stable cross section and then formulate an equation for  $a$  based on the variational stability of the scattering amplitude. Analysis of the solution of this equation shows that the scattering amplitude deduced from a fully converged solution of the SMC equation is independent of  $a$  even though the SMC operator itself is  $a$ -dependent. This seemingly paradoxical result arises from the fact that the role of  $a$  in the SMC equation is related to how the Lippmann-Schwinger and Schrödinger equations are combined. A fully converged solution should satisfy both the Lippmann-Schwinger and Schrödinger equations such that the result is independent of how the SMC operator is partitioned. In this respect, the variational stability of the scattering amplitude with respect to  $a$  furnishes a stringent test for the convergence of an SMC calculation. We note that in most variational calculations, such as the determination of scattering wave functions based on the stability of the scattering amplitude or phase shift, and bound state wave functions based on the stability of the total energy, the

solutions are generally unique. The solution of the  $a$ -equation is unusual in this respect because, for a converged calculation, it provides an infinite (but denumerable) number of solutions.

While the study of  $a$  for fully converged calculations is a purely formal exercise, for calculations using a finite basis, the present result is very useful in determining an optimal basis and testing convergence. In this respect, the test of  $a$ -invariance provides a unique window to the quality of the SMC calculations that apparently has no counterpart in other methods. It also furnishes a 'litmus' test for pseudo-resonances because pseudo-resonances are sensitive to the value of  $a$ . Finally, for studies using small to medium size basis sets, the global stability of the scattering cross section with respect to  $a$  may serve to expedite the convergence of the calculation.

In Sec. II, we review the SMC method and the original choice of  $a$  by Takatsuka and McKoy<sup>11,12</sup> based on the Hermiticity requirement of the principal-value SMC operator. We show that the principal-value SMC operator is Hermitian for arbitrary, real, and nonzero  $a$ . The matrix representation of the principal-value SMC operator is also Hermitian provided that the basis functions consist of either  $L^2$  functions and  $\delta$ -function orthonormalizable continuum functions, or purely  $L^2$  functions. However, if the continuum functions used are not  $\delta$ -function orthonormalizable, Takatsuka and McKoy's choice of  $a$  is one way to ensure Hermiticity. Hermiticity can also be achieved by two other means: iterating the projected Lippmann-Schwinger equation or enforcing a matrix element of  $E - H$  to be zero. In Sec. III we discuss the difference between an  $N$ -electron and an  $N + 1$ -electron projection operator and how the introduction of  $a$  is related to this difference. Based on the variational principle, an equation for  $a$  is derived in Sec. IV and the nature of its solutions is discussed. In two specific examples, elastic scattering in the static-exchange approximation and multichannel close-coupling calculations, the  $a$ -invariance is demonstrated by substituting converged wave functions from other methods into the SMC equation. Also, for the case of the lowest pole of  $H^-$ , we show that the SMC equation reduces to the Schrödinger equation and the solution is again independent of  $a$ . We then propose a search procedure to locate the region of  $a$ -invariance and establish a stable solution of the scattering amplitude. Two numerical examples are presented in Sec. V to illustrate the nature of the  $a$ -variation and the type of insight it can provide. Sec. VI concludes the paper.

## II. The projection parameter in the SMC method

The Hamiltonian for the electron + target system is given by

$$H = H_N + T_{N+1} + V, \quad (1)$$

where  $H_N$  is the target Hamiltonian,  $T_{N+1}$  is the kinetic energy operator for the continuum electron and  $V$  the interaction potential. In the SMC formulation, a projection operator  $P$ , originally introduced by Takatsuka and McKoy,<sup>11</sup> defines the open-channel space in terms of the eigenfunctions  $\Phi_m$  of the target Hamiltonian,

$$P = \sum_{m=1}^M |\Phi_m(1, 2, \dots, N)\rangle \langle \Phi_m(1, 2, \dots, N)|, \quad (2)$$

and

$$H_N |\Phi_m\rangle = E_m |\Phi_m\rangle. \quad (3)$$

The summation in Eq. (2) is over all energetically accessible target states. Notice that  $P$  is an  $N$ -electron projection operator, unlike the Feshbach projection operator<sup>28</sup> which is an  $N + 1$ -electron projection operator. In using  $P$  to partition the  $N+1$ -electron space, Takatsuka and McKoy multiply  $P$  by a projection parameter  $a$ .

$$\Psi_n^{(+)} = aP\Psi_n^{(+)} + (1 - aP)\Psi_n^{(+)}. \quad (4)$$

Here  $\Psi_n^{(+)}$  is an  $N+1$ -electron wave function. At this point the parameter  $a$  is arbitrary. Its variational determination is the subject of the present investigation. The dynamical equation in the  $aP$ -space is obtained from the projected Lippmann-Schwinger equation,

$$aP\Psi_n^{(+)} = aPS_n + aG_P^{(+)}V\Psi_n^{(+)}, \quad (5)$$

where  $S_n$  is the eigenfunction of the non-interacting Hamiltonian,  $H_N + T_{N+1}$ . The projected Green's function,  $G_P^{(+)}$ , with outgoing spherical wave boundary conditions, is defined in the open channel space by,

$$G_P^{(+)} = -\frac{1}{2\pi} \sum_{m=1}^M |\Phi_m\rangle \frac{\exp(ik_m |\vec{r}_{N+1} - \vec{r}_{N+1}'|)}{|\vec{r}_{N+1} - \vec{r}_{N+1}'|} \langle \Phi_m|. \quad (6)$$

The contribution from the complementary space is deduced from the Schrödinger equation.

$$(1 - aP)\hat{H}\Psi_n^{(+)} = 0. \quad (7)$$

$$\hat{H} = E - H. \quad (8)$$

The SMC equation is derived<sup>11</sup> by combining Eqs. (5) and (7) and multiplying by  $1/a$ ,

$$A^{(+)}\Psi_n^{(+)} = VPS_n, \quad (9)$$

where the SMC operator  $A^{(+)}$  with outgoing spherical wave boundary conditions is given by

$$A^{(+)} = \left\{ \frac{1}{2}(PV + VP) - VG_P^{(+)}V + \frac{1}{a}\hat{H} - \frac{1}{2}(P\hat{H} + \hat{H}P) \right\}, \quad (10)$$

Lima and McKoy<sup>29</sup> have demonstrated that the solution of Eq. (9) provides the complete wave function.

The Schwinger functional for the scattering amplitude, constructed from Eq. (9) is

$$f_{mn} = -\frac{1}{2\pi} \left\{ \langle S_m | V | \Psi_n^{(+)} \rangle + \langle \Psi_m^{(-)} | V | S_n \rangle - \langle \Psi_m^{(-)} | A^{(+)} | \Psi_n^{(+)} \rangle \right\}. \quad (11)$$

The principal-value SMC operator,  $A$ , is obtained by replacing  $G_P^{(+)}$  in Eq. (10) with the projected principal-value Green's function. Similarly, the wave functions in Eqs. (7), (9), and (11) should be replaced by those using standing wave boundary conditions. The principal-value operator was used in the original derivation of Takatsuka and McKoy, but most subsequent numerical calculations used  $A^{(+)}$ .

Takatsuka and McKoy,<sup>11,12</sup> and Lima and McKoy<sup>29</sup> argued that the variational stability of the Schwinger functional  $f_{mn}$  requires the principal-value SMC operator  $A$  to be Hermitian, or equivalently,  $A^{(+)\dagger} = A^{(-)}$ . While this condition is readily satisfied for trial functions consisting only of  $L^2$  functions, Takatsuka and McKoy noted that if the trial functions included (shielded) spherical Bessel and Neumann functions, the representation of  $A$  in this basis is generally non-Hermitian because the Hamiltonian matrix is non-Hermitian. In this case, the Hermiticity of the  $A$ -matrix is retrieved if the projection parameter is chosen to be

$$a = N + 1. \quad (12)$$

Equation (12) guarantees the following relationship to hold for the continuum portion of the open-channel functions,

$$\langle P\Psi_m | \frac{1}{a}\hat{H} - \frac{1}{2}(P\hat{H} + \hat{H}P) | P\Psi_n \rangle = 0. \quad (13)$$

Since the non-Hermitian part of the  $A$ -matrix involving continuum functions is identically zero, Eq. (12) ensures the Hermiticity of  $A$  in a basis which includes spherical Bessel and Neumann (or Hankel) functions.

Two aspects of Eq. (12) deserve further consideration. We note that Eq. (13) is also satisfied if

$$\langle P\Psi_m|\hat{H}|P\Psi_n\rangle = 0. \quad (14)$$

Thus even if the continuum functions in the basis results in a non-Hermitian  $H$ -matrix, the Hermiticity of  $A$  can be achieved using conditions other than Eq. (12). This point will be further considered in Sec. IV.

Another aspect of Takatsuka and McKoy's result is that, if the Hermiticity of  $A$  is used to determine  $a$ , the choice of  $a$  is basis set dependent and Eq. (12) is necessary if the basis set employed gives a non-Hermitian  $H$ -matrix. We note that the Hamiltonian operator, corresponding to a physical observable, must be Hermitian.<sup>30</sup> Furthermore, the Hermiticity of an operator depends only on the fact that it represents an observable, but not on its eigenvalue being in the discrete or continuum part of the spectrum. However, the continuum eigenfunction of a Hermitian operator must be  $\delta$ -function orthonormalizable.<sup>31</sup> In order to retain the Hermiticity in the matrix representation of  $H$ , the basis set used needs to be orthonormalizable either in terms of Kronecker  $\delta$ 's ( $L^2$  functions) or Dirac  $\delta$ -functions (continuum functions). However, in scattering calculations using Kohn or R-matrix methods, the phase shifts or T-matrices are deduced from the wavefunction at the asymptotic boundary. It is necessary to include both (shielded) spherical Bessel and Neumann functions in the trial basis. Such basis sets are not  $\delta$ -function orthonormalizable because the overlap integral between the (shielded) spherical Bessel and Neumann functions are not  $\delta$ -function representable. Consequently, the  $H$ -matrix in a basis containing such functions is non-Hermitian. This is a well recognized result from Kohn calculations. As noted earlier, the  $A$ -matrix in this basis is also non-Hermitian.

Through the use of Green's function, the solution of the Lippman-Schwinger equation automatically has the correct boundary condition. Thus the basis for the trial functions in a Schwinger calculation need not contain both spherical Bessel and Neumann functions. It can be a pure  $L^2$  basis or a  $L^2$  basis plus  $\delta$ -function orthonormalizable continuum functions. In this representation, the  $H$ -matrix is Hermitian. Even

if the initial trial basis is not properly orthonormalizable, Appendix A shows that the wave function from the next iteration in the Lippmann-Schwinger equation is again  $\delta$ -function orthonormalizable. Thus the iterative procedure can be used to ensure the Hermiticity property.

It remains to be shown that the operator  $A$  is Hermitian and the  $A$ -matrix, represented by a properly orthonormalizable basis, is also Hermitian. We recognize that  $\hat{H}$ ,  $V$ ,  $VG_PV$ , and  $P$  are all Hermitian operators. On the other hand, the product of two Hermitian operators need not be Hermitian. For example,  $P\hat{H}$  is not Hermitian because the operator  $P$ , defined in the  $N$ -electron space, and  $\hat{H}$ , defined in the  $N + 1$ -electron space, do not commute.<sup>32</sup> Thus the Hermiticity of  $A$  depends on the proof that both  $P\hat{H} + \hat{H}P$  and  $PV + VP$  are Hermitian. Consider two arbitrary  $N + 1$ -electron functions  $f$  and  $g$ , which can be properly orthonormalized.

$$\langle f|P\hat{H}|g\rangle = \sum_m \int d\vec{r}_{N+1} \langle f|\Phi_m\rangle_N \langle \Phi_m|\hat{H}|g\rangle_N. \quad (15)$$

The subscript  $N$  under the bra-ket sign denotes integration over the  $N$ -electron space.

$$\langle g|P\hat{H}|f\rangle^\dagger = \sum_m \int d\vec{r}_{N+1} \left( \langle g|\Phi_m\rangle_N \langle \Phi_m|\hat{H}|f\rangle_N \right)^\dagger = \langle f|\hat{H}P|g\rangle.$$

It is readily seen that

$$\langle g|P\hat{H} + \hat{H}P|f\rangle^\dagger = \langle f|P\hat{H} + \hat{H}P|g\rangle. \quad (16)$$

Thus  $P\hat{H} + \hat{H}P$  is Hermitian. The proof for  $PV + VP$  is similar. We conclude that  $A$  is a Hermitian *operator* independent of the choice of  $a$  as long as it is real. The  $A$ -matrix is also Hermitian in a basis which is  $\delta$ -function orthonormalizable. Under such circumstances, Eq. (12) is not necessary to maintain the Hermiticity of the  $A$ -matrix.

The present result demonstrates that, either by using a basis containing  $L^2$  functions plus  $\delta$ -function orthonormalizable continuum functions or purely  $L^2$  functions, or by using an iterative procedure to insure the orthonormalizability of the wave function, the Hermiticity of  $A$  is automatically satisfied. Then the Hermiticity requirement is insufficient to determine the parameter  $a$ , and  $a$  becomes a free parameter which can be chosen variationally so as to optimize the scattering calculation. This

is the approach used in the present study. Alternatively, one may include both the regular and irregular free-particle functions in the basis. Without iterating the projected Lippmann-Schwinger equation, this results in a non-Hermitian  $A$ -matrix. Either Eq. (12) or Eq. (14) can be used guarantee its Hermiticity. Finally, as in the complex Kohn approach, one may allow the  $A$ -matrix to be non-Hermitian. This will then allow the parameter  $a$  to be varied.

The use of a pure  $L^2$  basis requires further consideration. In the conventional form of the Schwinger variational principle, the Schwinger functional is given by

$$f_{mn} = -\frac{1}{2\pi} \left\{ \langle S_m | V | \Psi_n^{(+)} \rangle + \langle \Psi_m^{(-)} | V | S_n \rangle - \langle \Psi_m^{(-)} | V - VG^{(+)}V | \Psi_n^{(+)} \rangle \right\}.$$

All matrix elements in the above expression involve the operator  $V$ . If  $V$  is short range, then the long tail in the continuum portion of the trial function does not contribute to  $f_{mn}$  and it is justified to use a pure  $L^2$  basis in this type of variational principle. The Schwinger functional in the SMC method, Eq. (11), includes matrix elements of the kinetic energy operator. Takatsuka and McKoy<sup>11</sup> pointed out that, by setting  $a=N+1$ , the open channel matrix elements of the kinetic energy operator do not contribute to  $f_{mn}$  (see Eq. (13)), and a pure  $L^2$  basis again can be employed. In the present approach,  $a$  is treated as a variational quantity and Eq. (13) no longer holds. However, Appendix B shows that, for problems involving short range potentials, the matrix element in  $f_{mn}$  where the kinetic energy operator operates on purely continuum functions exactly cancels the difference between the total energy and the target energy.. The remaining matrix elements of the kinetic energy operator always include a bound function in the integrand and the continuum character of the trial basis is again unimportant. Consequently, even if  $a \neq N + 1$  it is justified to use a pure  $L^2$  basis for this type of variational principle.

### III. $N$ -electron and $N+1$ -electron projection operators

Before deriving a variational equation for  $a$ , it is worthwhile to consider first the difference between an  $N$ -electron and  $N+1$ -electron projection operator. The introduction of  $a$  originates from this difference. The Feshbach projection operator,<sup>28</sup> which operates on the total  $N+1$ -electron system, is defined without any extraneous parameters.

$$P_{N+1} = \sum_m |\Psi_m(1, 2, \dots, N, N+1)\rangle \langle \Psi_m(1, 2, \dots, N, N+1)| \quad (17)$$

Here  $m$  sums over the open channel functions. If  $\Psi_i$  is an open channel function,

$$P_{N+1}\Psi_i = \Psi_i. \quad (18)$$

On the other hand, when the  $N$ -electron operator  $P$ , defined in Eq. (2), operates on an  $N+1$ -electron wave function, the antisymmetric nature of fermion wave functions causes the result to be more complicated than Eq. (18). Consider the simplest case when the target wave function  $\Phi_i$  is expressible in terms of a closed shell, single determinantal wave function,

$$\Phi_i(1, 2, \dots, N) = \mathcal{A} \left\{ \phi_1\alpha(1)\phi_1\beta(2)\dots\phi_{N/2}\alpha(N-1)\phi_{N/2}\beta(N) \right\}. \quad (19)$$

Here  $\alpha$  and  $\beta$  denote spin functions. If the wave function of the continuum electron,  $f_i(N+1)$ , is orthogonal to all the target orbitals, then the  $S_z = 1/2$  component of  $\Psi_i$  becomes

$$\Psi_i(1, 2, \dots, N, N+1) = \mathcal{A} \left\{ \phi_1\alpha(1)\phi_1\beta(2)\dots\phi_{N/2}\beta(N)f_i\alpha(N+1) \right\}, \quad (20)$$

We have

$$P\Psi_i(1, 2, \dots, N, N+1) = \frac{1}{\sqrt{N+1}}\Phi_i(1, 2, \dots, N)f_i\alpha(N+1), \quad (21)$$

and

$$\langle \Psi_j | HP | \Psi_i \rangle = \frac{1}{N+1} \langle \Psi_j | H | \Psi_i \rangle. \quad (22)$$

A comparison of Eqs. (18) and (21) clearly shows the origin of the projection parameter. When an  $N$ -electron projection operator is applied to an  $N+1$ -electron wave function,

a projection parameter needs to be introduced to account for the difference between  $N$ -electron and  $N+1$ -electron antisymmetrization. Using Eq. (22) it is straightforward to derive the result of Takatsuka and McKoy<sup>11</sup> for elastic scattering in the static-exchange approximation using a closed shell SCF target function or an open shell target function with a simple spin coupling scheme.

Eq. (21) is not applicable when the orthogonality constraint between the continuum electron wave function and the target wave function is relaxed, and/or when the target is described by more sophisticated wave functions. Consider the simple case of  $X^1\Sigma_g^+ \rightarrow b^3\Sigma_u^+$  excitation of  $H_2$  by electron impact. Let the wave function for the  $X^1\Sigma_g^+$  state be represented by

$$\Phi_x = \mathcal{A}\{1\sigma_g\alpha(1)1\sigma_g\beta(2)\} \quad (23a)$$

and the three spin components of the  $b^3\Sigma_u^+$  state by

$$\Phi_{b1} = \mathcal{A}\{1\sigma_g\alpha(1)1\sigma_u\alpha(2)\} \quad (23b)$$

$$\Phi_{b0} = \mathcal{A}\left\{1\sigma_g(1)1\sigma_u(2)\frac{1}{\sqrt{2}}(\alpha(1)\beta(2) + \beta(1)\alpha(2))\right\} \quad (23c)$$

$$\Phi_{b-1} = \mathcal{A}\{1\sigma_g\beta(1)1\sigma_u\beta(2)\} \quad (23d)$$

It is well established that in calculating this transition, correlation terms of the form

$$\Psi_a = \mathcal{A}\{1\sigma_g\alpha(1)1\sigma_u\alpha(2)1\sigma_u\beta(3)\}, \quad (24a)$$

and

$$\Psi_b = \mathcal{A}\{1\sigma_g\alpha(1)1\sigma_g\beta(2)1\sigma_u\alpha(3)\}, \quad (24b)$$

should be included. These are usually called ‘penetration’ or ‘recorrelation terms’ in other methods because they relax the enforced orthogonality between the continuum and target functions. Let the projection operator  $P$  be generated from the four target functions in Eqs. (23a-d). We then have

$$P\Psi_a = \frac{1}{\sqrt{3}}\Phi_{b1}(1,2)1\sigma_u\beta(3) - \frac{1}{\sqrt{6}}\Phi_{b0}(1,2)1\sigma_u\alpha(3). \quad (25)$$

This simple example illustrates the fact that, when the SMC method is applied to problems other than static-exchange scattering with simple target functions, the rationale of setting  $a = N+1$ , based on Eq. (21), is not valid.

While the use of an  $N$ -electron projection operator leads to the introduction of a projection parameter, it does have significant advantages in retaining a simple representation of the projected Green's function, Eq. (6). Note that the use of the Feshbach operator results in a much more complicated expression for the projected Green's function because of the nonorthogonality between the continuum and target functions. Furthermore, an  $N$ -electron projection operator obviates the need for orthogonality constraints between the continuum and target functions. The method has built-in nonorthogonality because the plane waves in the homogeneous solution  $S_n$  and Green's function  $G_P^{(+)}$  are not orthogonalized to the target functions. Thus  $\Psi_a$  and  $\Psi_b$  in Eqs. (24a,b) act as correlation terms in the SMC method whereas in other methods they play dual roles of correlation and penetration functions. In addition, the complementary space in the SMC method is directly constructed from  $1-aP$ . In contrast, some applications of the optical potential method construct the complementary space separately from the  $P$ -space. These advantages of the SMC method cannot be over emphasized.

#### IV. Variational determination of $a$

Sec. II shows that, by choosing a properly orthonormalizable basis, or by iterating the projected Lippmann-Schwinger equation,  $a$  becomes a free parameter. An optimal choice of  $a$  should then be derived variationally. To demonstrate that  $a$  indeed acts as a free parameter, consider using as a trial function the converged static-exchange wave function obtained using another method.

$$\Psi_{SE} = \mathcal{A}\Phi_o(1, \dots, N)f_{SE}(N+1), \quad (26)$$

$$(h_{SE} - \frac{1}{2}k^2)f_{SE} = 0, \quad (27a)$$

and

$$\langle \Psi_{SE} | \hat{H} | \Psi_{SE} \rangle = 0. \quad (27b)$$

Since  $\Psi_{SE}$  contains only open channel functions,

$$\langle \Psi_{SE} | P \hat{H} | \Psi_{SE} \rangle = \langle \Psi_{SE} | \hat{H} P | \Psi_{SE} \rangle = 0. \quad (27c)$$

We have

$$\langle \Psi_{SE} | A | \Psi_{SE} \rangle = \langle \Psi_{SE} | \frac{1}{2}(PV + VP) - VG_P V | \Psi_{SE} \rangle. \quad (28)$$

The resulting  $A$ -matrix is  $a$ -independent. Also, Eqs. (27b,c) are equivalent to Eq. (14) and the Hermitian representation of  $A$  is guaranteed.

For the second example, consider the trial function obtained from a close coupling calculation (which may include closed channel functions),

$$\langle \Psi_{CC} | \hat{H} | \Psi_{CC} \rangle = 0. \quad (29)$$

$$\langle \Psi_{CC} | A | \Psi_{CC} \rangle = \langle \Psi_{CC} | \frac{1}{2}(PV + VP) - VG_P V - \frac{1}{2}(P\hat{H} + \hat{H}P) | \Psi_{CC} \rangle. \quad (30)$$

The  $a$ -dependence disappears. Since Eq. (14) may not be satisfied, whether  $A$  in this representation is Hermitian or not depends on the original basis used for  $\Psi_{CC}$ .

As a third examples, consider calculation of the lowest pole of  $H^-$ . In this case the open channel space is null.

$$P = 0.$$

The SMC equation in Eq. (9) is reduced to

$$\frac{1}{a} \hat{H} \Psi_n = 0.$$

Here  $\frac{1}{a}$  is just overall multiplicative factor which can be discarded. We then retrieve the Schrödinger equation, independent of  $a$ .

The above examples demonstrate that the choice  $a = N + 1$  is not unique. Except in the bound state case where  $a$  drops out completely, a variational determination of  $a$  is generally preferable. Here we consider the simultaneous optimizations of  $a$  together with the trial scattering functions. Let  $\Psi_n^{(+)}$  and  $\Psi_m^{(-)}$  be expanded in a set of trial functions  $f_r$ ,

$$|\Psi_n^{(+)}\rangle = \sum_r b_r(\vec{k}_n) |f_r\rangle, \quad (31)$$

and

$$\langle \Psi_m^{(-)} | = \sum_s c_s(\vec{k}_m) \langle f_s|. \quad (32)$$

The Schwinger functional is now written as

$$f_{mn} = -\frac{1}{2\pi} \left[ \sum_r b_r \langle S_m | V | f_r \rangle + \sum_s c_s \langle f_s | V | S_n \rangle - \sum_r \sum_s b_r c_s \langle f_s | A^{(+)} | f_r \rangle \right]. \quad (33)$$

The requirement that  $f_{mn}$  be stationary with respect to first order variations in  $b_r$ ,  $c_s$ , and  $a$ ,  $\partial f_{mn} / \partial b_r = 0$ ,  $\partial f_{mn} / \partial c_s = 0$ ,  $\partial f_{mn} / \partial a = 0$ , gives the following relationships,

$$\langle S_m | V | f_r \rangle - \sum_s c_s \langle f_s | A^{(+)} | f_r \rangle = 0, \quad (34)$$

$$\langle f_s | V | S_n \rangle - \sum_r b_r \langle f_s | A^{(+)} | f_r \rangle = 0, \quad (35)$$

and

$$\sum_r \sum_s b_r c_s \langle f_s | \hat{H} | f_r \rangle = 0. \quad (36)$$

The solutions for  $b_r$ ,  $c_s$  are<sup>33</sup>

$$b_r = \sum_s D_{rs} \langle f_s | V | S_n \rangle, \quad (37a)$$

$$c_s = \sum_r \langle S_m | V | f_r \rangle D_{rs}, \quad (37b)$$

with

$$(D^{-1})_{rs} = \langle f_r | A^{(+)} | f_s \rangle. \quad (38)$$

Notice that in the expression for  $(D^{-1})_{rs}$ , the parameter  $a$  appearing in  $A^{(+)}$  is still undetermined. Substitute Eqs. (37a,b) into Eq. (36), we get

$$\sum_r \sum_s \sum_t \sum_{t'} \langle S_m | V | f_t \rangle D_{ts} \langle f_s | \hat{H} | f_r \rangle D_{rt'} \langle f_{t'} | V | S_n \rangle = 0. \quad (39)$$

Eq. (39) is an algebraic equation for  $a$ . Using the value of  $a$  determined from Eq. (39) to evaluate  $D$ , we obtain a variationally stable expression for  $f_{mn}$ ,

$$f_{mn} = -\frac{1}{2\pi} \sum_{rs} \langle S_m | V | f_r \rangle D_{rs} \langle f_s | V | S_n \rangle. \quad (40)$$

This expression of  $f_{mn}$  is identical with those obtained by Takatsuka and McKoy,<sup>11,12</sup> except for the value of  $a$  used.

Equation (39) provides variationally optimal values of  $a$ . It is a high-order algebraic equation, the order being proportional to the number of trial functions used. A number of useful properties of the solution can be deduced by studying the structure of Eq. (39):

- (1) If the trial functions are the variational solutions of the Schrödinger equation,

$$\langle f_s | \hat{H} | f_r \rangle = 0,$$

then Eq. (39) will be satisfied independent of the choice of  $a$ . This is a physically intuitive result and has already been illustrated by the first two examples cited in the beginning of this section.

(2) The solution depends on the initial and final channels under study. Thus in a multichannel calculation, different  $a$ 's will be used for elastic, superelastic, and inelastic scattering.

- (3) For a given transition, the value of  $a$  depends on the trial functions used.

(4) If a complete basis is used, the result should be independent of the choice of  $a$ . This comes from property (1) and the invariance of Eq. (39) to a unitary transformation.

It is important to note that the term basis denotes both the basis set used to expand the one-electron functions, e.g., a Gaussian basis set, and the  $N+1$ -electron basis that describes the multichannel nature of the wave function, i.e., the open and closed channel functions. This property is found to be very useful in testing the completeness of the basis used.

(5) The solution of Eq. (39) depends on both the energy and direction of the incident and scattered electrons. However, if we consider the following operator equation,

$$\sum_r \sum_s \sum_t \sum_{t'} V|f_t\rangle D_{ts} \langle f_s | \hat{H} | f_r \rangle D_{rt'} \langle f_{t'} | V = 0, \quad (41)$$

the  $a$ 's which satisfy Eq. (41) will automatically satisfy Eq. (39). They represent a subset of the solutions of Eq. (39) which are independent of the direction of the incident and scattered electrons. Also, the  $a$ 's determined in this manner satisfy both  $\partial f_{mn}/\partial a = 0$  and  $\partial \sigma_{mn}/\partial a = 0$ , with  $\sigma_{mn}$  denoting the integral cross section.

In general, the dimensionality of Eqs. (39) and (41) makes a direct solution difficult in practical problems. Alternatively, a search procedure can be used. Starting with a trial value of  $a$ , the matrix elements of  $A^{(+)}$  can be determined and the scattering amplitude  $f_{mn}$  calculated using Eq. (40). The parameter  $a$  is then varied to search for optimal values. Also, we combine the search for the stability of  $f_{mn}$  with a test of the adequacy of the basis (property 4) by looking for solutions where  $f_{mn}$  or  $\sigma_{mn}$  is invariant to  $a$ . Numerical examples using this technique are presented in the next section.

## V. Numerical Examples

As an illustration, we studied e-CO elastic scattering in the static-exchange approximation. The calculation uses an uncontracted  $\{C10s6p1d|O10s6p1d|CM2s3p1d\}$  basis with  $CM$  denoting the center of mass. The C and O basis start with the  $9s5p$  basis of Huzinaga<sup>34</sup> supplemented with one diffuse  $s$  and one diffuse  $p$  functions, with exponents 0.04736 and 0.03654 for C and 0.08619 and 0.06368 for O. The  $d$  exponents for C and O are the recommended values of Dunning.<sup>35</sup> The exponents for the center of mass functions are selected from the table of Nestman and Peyerimhof.<sup>36</sup> They are 0.032426 and 0.009211 for  $s$ , 0.041975, 0.01997, and 0.009467 for  $p$ , and 0.04349 for  $d$ . All calculations were carried out at the internuclear distance of 2.132  $a_0$ .

Sec. IV shows that the SMC static-exchange result should be independent of  $a$  if the one-electron basis has converged. Fig. 1a and b present the integral cross sections at 3.75 eV incident energy as a function of  $a$ , for  $a = 10 - 20$  in steps of 0.1. (The value of  $a$  is 15 if it is set to  $N + 1$ ). Of 100 points calculated, 81 fall within 5% of each other, as depicted in Fig. 1a. Fig. 1b shows the full calculation where a number of significant oscillations in the cross sections are shown. These instabilities are a direct consequence of the incompleteness of the basis used. The result of the  $a$  variation means that the basis set is probably adequate if 95% accuracy in the cross section is acceptable.

The source of the sharp peaks and dips in Fig. 1b is analogous to the pseudo-resonances in the Schwinger method reported by Apagyi et al.<sup>37</sup> and analyzed by Weatherford et al.<sup>38</sup> and by Winstead and McKoy.<sup>39</sup> When the basis for expanding the wave function is complete, the matrices of  $\hat{H}$ ,  $P\hat{H}$  and  $\hat{H}P$  all have zero eigenvalues and the eigenvalues of  $A^{(+)}$  in this representation do not go to zero unless a real resonance exists. On the other hand, the matrix of  $\hat{H}$  represented by an incomplete basis generally does not have zero eigenvalues. Thus a particular choice of  $a$  may cause a near cancelation between  $\hat{H}/a$  and the remaining terms in  $A^{(+)}$  such that  $A^{(+)}$  has an eigenvalue close to zero. Similarly, a dip indicates a corresponding maximum eigenvalue of  $A^{(+)}$ . Notice the sharpness of these structures, a characteristic of pseudo-resonances. Since  $\partial\sigma_{mn}/\partial a = 0$  is also satisfied at these structures, we consider a choice of  $a$  based on the flatness of the cross section vs  $a$  curve to be superior to the simple condition  $\partial\sigma_{mn}/\partial a = 0$ .

As a second example, we studied the effect of the variation of  $a$  on the  $e\text{-H}_2$ ,  $X^1\Sigma_g^+ \rightarrow b^3\Sigma_u^+$  excitation cross sections using a two-state approximation. This is a well studied transition; calculations using the SMC,<sup>15,20</sup> R-matrix,<sup>40,41</sup> linear algebraic,<sup>42,43</sup> and S-matrix Kohn<sup>6,44</sup> methods have been reported. These calculations showed that the correlation/penetration terms such as those given in Eqs. (24a,b) are important in describing the scattering process.

Two Gaussian basis sets were used. The 64-basis, consisting of 64 uncontracted Gaussian functions, is a {H6s6p|CM4s4p} set that was used in the original calculations of Lima et al<sup>15,20</sup> and the cross sections are in good agreement with experiment.<sup>45-47</sup> The 70-basis, composed of 70 uncontracted Gaussians, is a {H8s7p|CM3s3p} set which employs the s and p functions from van Duijneveldt's<sup>48</sup> 8s6p4d hydrogen basis, supplemented with one p function (exponent 0.03125) at the nuclear centers, and three s functions (exponents 0.082, 0.021, 0.0052) and three p functions (exponents 0.114, 0.0226, 0.0045) at the center of mass. The hydrogen basis of van Duijneveldt, in the form of atomic natural orbitals, has been used frequently in high quality quantum chemical calculations of hydrides and their ions.<sup>49</sup> Based on previous experience, we expect the 70-basis to be superior to the 64-basis. The present study employs the same type of target functions as previous SMC calculations on this transition,<sup>15,20</sup> i.e., an SCF function for the ground state and an IVO function<sup>50</sup> for the  $b$  state, so that the  $a$ -dependence of the cross section would not be attributed to the difference in the target wave functions. All calculations were carried out at a bond length of 1.4  $a_0$  using the AMES SMC code. We determined the integral cross sections as a function of both  $a$  and the electron energy. The range of  $a$  used is 2.0 - 4.0 in steps of 0.05. Also note that the results of the 64-basis calculations are slightly different from Lima et al.<sup>20</sup> because a better representation of the  $VG_p^{(+)}V$  term is used.

Analogous to the CO static-exchange result, the  $e\text{-H}_2$  elastic cross sections versus  $a$  curve also show regions of stability, with sharp structures between stable regions. Figs. 2a and 2b depict the elastic cross sections at 13 eV, calculated using the 70-basis and 64-basis, respectively. Only the data points within 10% of each other are depicted. For the 70-basis, 72.5% of the data points satisfy this criterion, versus 45% for the 64-basis. From this point of view, the 70-basis is superior, even though the cross section averaged over the converged data points, shown as a dashed line in the figures, is in agreement with each other, 23.4 au for the 70-basis and 22.8 au for the 64-basis. Even for the

70-basis, the convergence is inferior to the CO result. We consider this a consequence of the inadequacy of the  $N + 1$ -electron basis used in the two-channel calculation, and not due to an inferior one-electron basis. Note that the  $N + 1$ -electron basis (multichannel) does not play a role in the static-exchange approximation used in the CO calculation.

Figures 3a and 3b depict the inelastic cross sections from the 70-basis and 64-basis calculations where the data points are within 10% of each other. Among the calculated values, 45% and 50%, respectively, fall in this range. Thus for the 70-basis the convergence of the inelastic cross sections is significantly inferior to the elastic case whereas the quality of the 64-basis cross sections remain roughly the same. The 70-basis result serves as an indication that an optimal basis for elastic and inelastic calculations may be different.

Note that for the 64-basis, the regions of stability for both elastic and inelastic cross sections include the point at  $a=3.0$ , corresponding to Takatsuka and McKoy's choice of  $N + 1$ , whereas the cross section at this  $a$  is not in the set of converged points for the 70-basis. Fig. 4 compares the inelastic cross section as a function of electron energy, for the 64-basis and 70-basis at  $a = 3.0$ , and the 70-basis cross sections determined using the average of the converged cross sections at each energy. Experimental data<sup>45-47</sup> for this transition are also included for comparison. Note that the 64-basis cross sections at  $a=3.0$  and the average cross section from the 70-basis calculations are in agreement with experiment and with each other to within the estimated errors, but the 70-basis cross section curve at  $a=3.0$  differs significantly in both shape and magnitude from the other two curves and from experiment. In particular, the experimental data show no evidence of a dip around 16 eV. If  $a = N + 1$  is considered a unique choice, we have the paradoxical result that a larger and, generally considered better, basis gives cross sections that disagree not only with the previous SMC results, but also with calculations using other methods and with experiment. However, if we accept  $a$  as a variational parameter and the optimal cross section using  $a$ -stability criteria, then the 70-basis results agree with the generally accepted values. This numerical example demonstrates the importance of  $a$ -variation.

All previous reported SMC cross sections<sup>13-26</sup> were calculated using  $a = N+1$ . From our point of view, this is just one of many possible values of  $a$ . In general, a calculation of the cross section vs  $a$  curve is recommended since it provides both a con-

vergence test and a ready check for pseudo-resonances. Furthermore, the requirement that the cross section curve be flat with respect to  $a$  provides a variationally more meaningful cross section than calculations using one single value of  $a$ .

## VI. Conclusions

This study considers the role of the projection parameter in the SMC method and develops a variational equation for it. While the multiple solutions in the variational equation may at first appear to be a disadvantage, it actually provides a sensitive test of the convergence when we couple the variational solution of  $a$  with the requirement that, for a fully converged calculation, the cross section is invariant with  $a$ . The convergence requirement applies both to the one-electron and  $N+1$ -electron basis. Such a test is apparently unique to the SMC method. It is also shown that calculations using an incomplete basis, as is the case in all practical calculations, may find pseudo-resonances when the choice of  $a$  causes the SMC operator to have a near zero eigenvalue. Thus it is essential to test the stability of the cross sections with the  $a$ -variation. Studies on the invariance of the cross section with  $a$  using more sophisticated target wave functions and more extensive multichannel treatments are under way.

## Acknowledgements

We would like to thank Drs. T. N. Rescigno, B. Lengsfield, and Prof. C. W. McCurdy for helpful discussions and Dr. Robert K. Nesbet for a discussion on the different basis set requirements of the Kohn and Schwinger methods. C.A.W. would like to acknowledge the support of NASA Ames Cooperative Agreement No. NCC 2-492 and a grant of computer time on the Florida State University CRAY-YMP.

Appendix A. Orthonormalizability of the iterative solutions of  
the projected Lippmann-Schwinger equation

Consider the projected Lippmann-Schwinger equation

$$P\Psi^{(+)} = \varphi^{(+)} + G_P^{(+)}V\Psi_t^{(+)}, \quad (A-1)$$

where  $\varphi^{(+)}$  is the projected homogeneous solution and satisfies the  $\delta$ -function orthonormalization condition,

$$\langle \varphi_1^{(+)} | \varphi_2^{(+)} \rangle = \delta(\vec{k}_1 - \vec{k}_2). \quad (A-2)$$

In Eq. (A-1),  $\Psi_t^{(+)}$  is the wave function represented in the initial trial basis and  $\Psi^{(+)}$  is the wave function after one iteration of the projected Lippmann-Schwinger equation. The initial trial basis may be composed of purely  $L^2$  functions or  $L^2$  plus continuum functions. If continuum functions are included in the basis,  $\delta$ -function orthonormalizability is not required. Consider the overlap integral

$$\begin{aligned} \langle P\Psi_1^{(+)} | P\Psi_2^{(+)} \rangle &= \langle \varphi_1^{(+)} | \varphi_2^{(+)} \rangle + \langle \varphi_1^{(+)} | G_P^{(+)}(E_2)V\Psi_{2t}^{(+)} \rangle \\ &+ \langle G_P^{(+)}(E_1)V\Psi_{1t}^{(+)} | \varphi_2^{(+)} \rangle + \langle G_P^{(+)}(E_1)V\Psi_{1t}^{(+)} | G_P^{(+)}(E_2)V\Psi_{2t}^{(+)} \rangle. \end{aligned} \quad (A-3)$$

Direct integration gives

$$\langle \varphi_1^{(+)} | G_P^{(+)}(E_2)V\Psi_{2t}^{(+)} \rangle = \lim_{\delta \rightarrow 0} \frac{1}{E_2 - E_1 + i\delta} \langle \varphi_1^{(+)} | V | \Psi_{2t}^{(+)} \rangle. \quad (A-4)$$

$$\langle G_P^{(+)}(E_1)V\Psi_{1t}^{(+)} | \varphi_2^{(+)} \rangle = \lim_{\delta \rightarrow 0} \frac{1}{E_1 - E_2 + i\delta} \langle \Psi_{1t}^{(+)} | V | \varphi_2^{(+)} \rangle. \quad (A-5)$$

and

$$\begin{aligned} &\langle G_P^{(+)}(E_1)V\Psi_{1t}^{(+)} | G_P^{(+)}(E_2)V\Psi_{2t}^{(+)} \rangle \\ &= \lim_{\delta \rightarrow 0} \frac{1}{E_1 - E_2 + 2i\delta} [\langle G_P^{(+)}(E_1)V\Psi_{1t}^{(+)} | V | \Psi_{2t}^{(+)} \rangle - \langle \Psi_{1t}^{(+)} | V | G_P^{(+)}(E_2)V\Psi_{2t}^{(+)} \rangle]. \end{aligned} \quad (A-6)$$

Combining Eqs. (A-2), (A-4), (A-5), and (A-6) and taking the limit  $\delta = 0$ , we find

$$\langle P\Psi_1^{(+)} | P\Psi_2^{(+)} \rangle = \delta(\vec{k}_1 - \vec{k}_2) + \frac{1}{E_2 - E_1} [\langle P\Psi_1^{(+)} | V | \Psi_{2t}^{(+)} \rangle - \langle \Psi_{1t}^{(+)} | V | P\Psi_2^{(+)} \rangle]. \quad (A-7)$$

The presence of the interaction potential  $V$ , which vanishes at least like  $r^{-1}$  as  $r \rightarrow \infty$ , guarantees that the last two matrix elements in Eq. (A-7) do not diverge for neutral,

bound target functions even if  $\Psi_{1t}^{(+)}$  and  $\Psi_{2t}^{(+)}$  are represented in a basis including continuum functions which are not  $\delta$ -function normalizable. Eq. (A-7) means that  $P\Psi_1^{(+)}$ , and hence  $\Psi_1^{(+)}$ , are  $\delta$ -function orthonormalizable. Thus the iterative solution of the projected Lippmann-Schwinger equation is  $\delta$ -function orthonormalizable even if the initial trial function is not.

$$\begin{aligned}
& \div (-1)^{P_3} \int d\vec{r}_1 d\vec{r}_2 d\vec{r}_3 d\vec{r}'_3 D_{mn}^{(3)}(\vec{r}_1 \vec{r}_2 \vec{r}_3, \vec{r}_1 \vec{r}_2 \vec{r}'_3) \frac{1}{|\vec{r}_1 - \vec{r}_2|} s_{\lambda_m}^\dagger(k_m r'_3) Y_{\lambda_m \mu_m}^\dagger(\hat{r}'_3) \\
& \quad \times s_{\lambda_n}(k_n r_3) Y_{\lambda_n \mu_n}(\hat{r}_3) \tag{B-4}
\end{aligned}$$

The first term on the right hand side of Eq. (B-4) vanishes due to Eq. (B-2). The second term involves the short range potential  $V$  which does not weigh the long range part of  $s_{\lambda_m}$  and  $s_{\lambda_n}$ . The last three terms on the rhs of Eq. (B-4) comes from the non-orthogonality between the target functions and the spherical Bessel functions. The transition one-, two- and three-particle density of target functions  $\Phi_m$  and  $\Phi_n$  are denoted by  $D_{mn}^{(1)}$ ,  $D_{mn}^{(2)}$ , and  $D_{mn}^{(3)}$ ,  $P_1$ ,  $P_2$  and  $P_3$  represent the number of permutation operations, and  $U(\vec{r})$  the nuclear attraction potential. Note that all target transition density functions are short-range. Thus the last three integrals in Eq. (B-4) involving short-range integrands in all coordinates. The long tail of the continuum functions  $s_{\lambda_m}$  and  $s_{\lambda_n}$  again does not contribute to these matrix elements. It is straightforward to show that similar conclusions apply to matrix elements of  $P\hat{H}$  and  $\hat{H}P$ .

In view of the above result, the matrix elements in the Schwinger functional in Eq. (11) is insensitive to the continuum nature of the trial function even when  $a \neq N+1$  and Eq. (13) does not apply. This justifies the use of pure  $L^2$  basis in the variational principle developed in this paper.

## References

1. L. Hulthén, Kgl. Fysiograf. Sällskap. Lund. Fröh. 14, 257 (1944).
2. W. Kohn, Phys. Rev. 74, 1763 (1958).
3. S. I. Rubinow, Phys. Rev. 96, 218 (1954).
4. R. K. Nesbet, *Variational Methods in Electron – Atom Scattering*, (Plenum, New York, 1980).
5. W. H. Miller and B. M. D. D. Jansen op de Haar, J. Chem. Phys. 86, 6213 (1987).
6. B. I. Schneider and T. N. Rescigno, Phys. Rev. A37, 3749 (1988).
7. P. G. Burke and W. D. Robb, Adv. Atom. Mol. Phys. 11, 144 (1975).
8. J. Schwinger, Phys. Rev. 72, 742 (1947).
9. R. G. Newton, *Scattering Theory of Waves and Particles*, 2nd Edition, (Springer-Verlag, New York, 1982).
10. D. K. Watson, Adv. Atom. Mol. Phys. 25, 221 (1988).
11. K. Takatsuka and V. McKoy, Phys. Rev. A24, 2473 (1981).
12. K. Takatsuka and V. McKoy, Phys. Rev. A30, 1734 (1984).
13. T. L. Gibson, M. A. P. Lima, K. Takatsuka, and V. McKoy, Phys. Rev. A30, 3005 (1984).
14. M. A. P. Lima, T. L. Gibson, W. M. Huo, and V. McKoy, Phys. Rev., A32, 2696 (1985).
15. M. A. P. Lima, T. L. Gibson, W. M. Huo, and V. McKoy, J. Phys., B18, L865 (1985).
16. L. M. Brescansin, M. A. P. Lima, T. L. Gibson, V. McKoy, and W. M. Huo, J. Chem. Phys., 85, 1854 (1986).

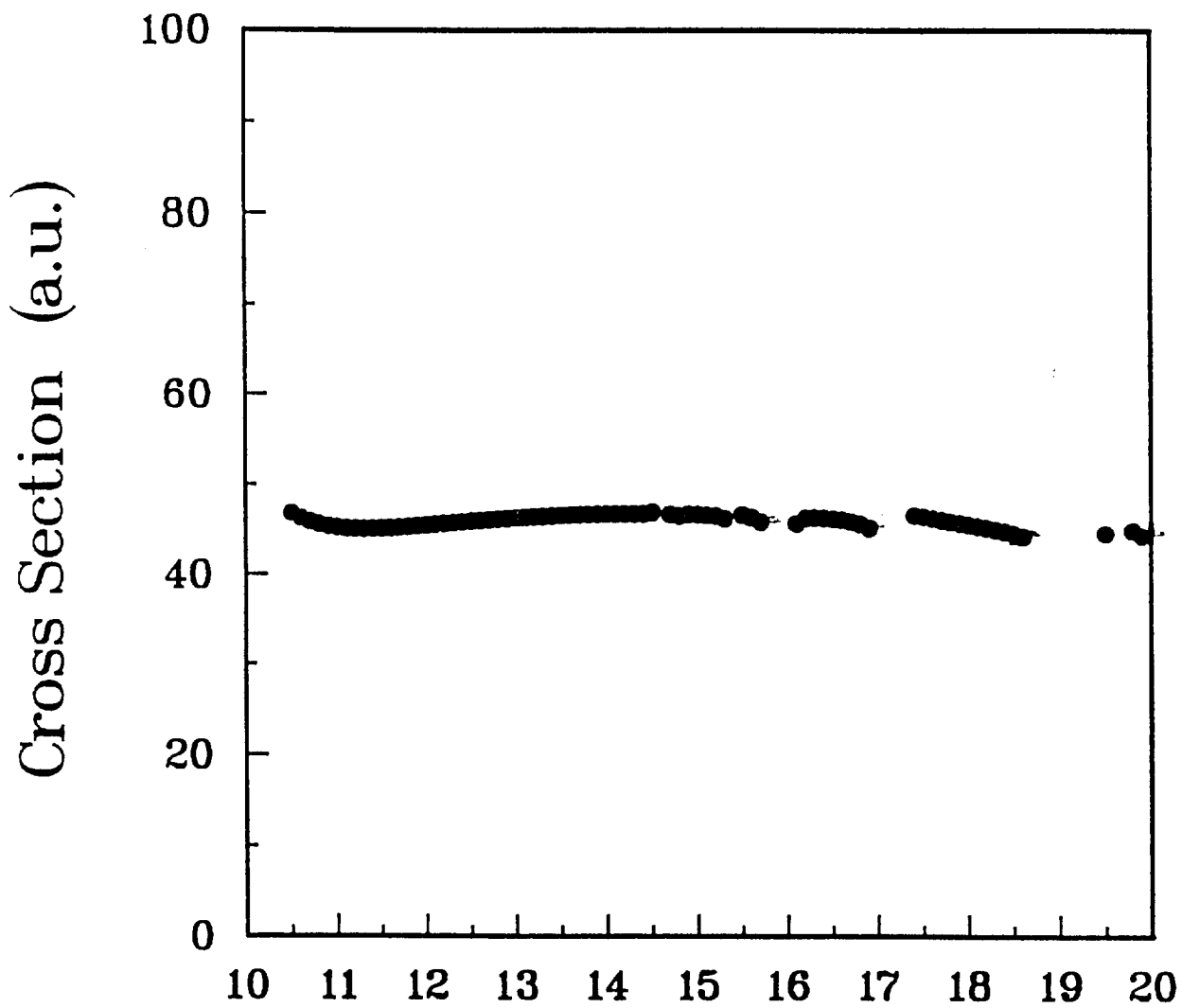
17. W. M. Huo, T. L. Gibson, M. A. P. Lima, and V. McKoy, Phys. Rev., A36, 1632 (1987).
18. W. M. Huo, M. A. P. Lima, T. L. Gibson, and V. McKoy, Phys. Rev., A36, 1642 (1987).
19. T. L. Gibson, M. A. P. Lima, V. McKoy, and W. M. Huo, Phys. Rev., A35, 2473 (1987).
20. M. A. P. Lima, T. L. Gibson, V. McKoy, and W. M. Huo, Phys. Rev. A38, 4527 (1988).
21. W. M. Huo, Phys. Rev., A38, 3303 (1988).
22. H. P. Pritchard, M. A. P. Lima, and V. McKoy, Phys. Rev. A39, 2392 (1989).
23. M. A. P. Lima, K. Watari, and V. McKoy, Phys. Rev. A39, 4312 (1989).
24. C. A. Weatherford and W. M. Huo, Phys. Rev., A41, 186 (1990).
25. W. M. Huo, *Nonequilibrium Processes in Partially Ionized Gases*, M. Capitelli and J. N. Bardsley, editors, NATO Advanced Study Institute Series, p. 341 Plenum (1990).
26. C. Winstead and V. McKoy, Phys. Rev. A42, 5357 (1990).
27. C. Winstead, P. G. Hipes, M. A. P. Lima, and V. McKoy, J. Chem. Phys. 94, 5455 (1991).
28. H. Feshbach Ann. Phys. 19, 287 (1962).
29. M. A. P. Lima and V. McKoy, Phys. Rev. A 38, 501 (1988).
30. C. J. Joachain, *Quantum Collision Theory* North Holland, Amsterdam (1983), p. 660.
31. A. Messiah, *Quantum Mechanics* Vol. I, John Wiley, New York (1961), Chapter VII, Sec. 9. See in particular the discussions in pp. 185-186.

49. J. Almlöf and P. R. Taylor, Adv. Quantum Chem. (in press).
50. W. J. Hunt and W. A. Goddard III, Chem. Phys. Lett. 3, 414 (1969).

**PRECEDING PAGE BLANK NOT FILMED**

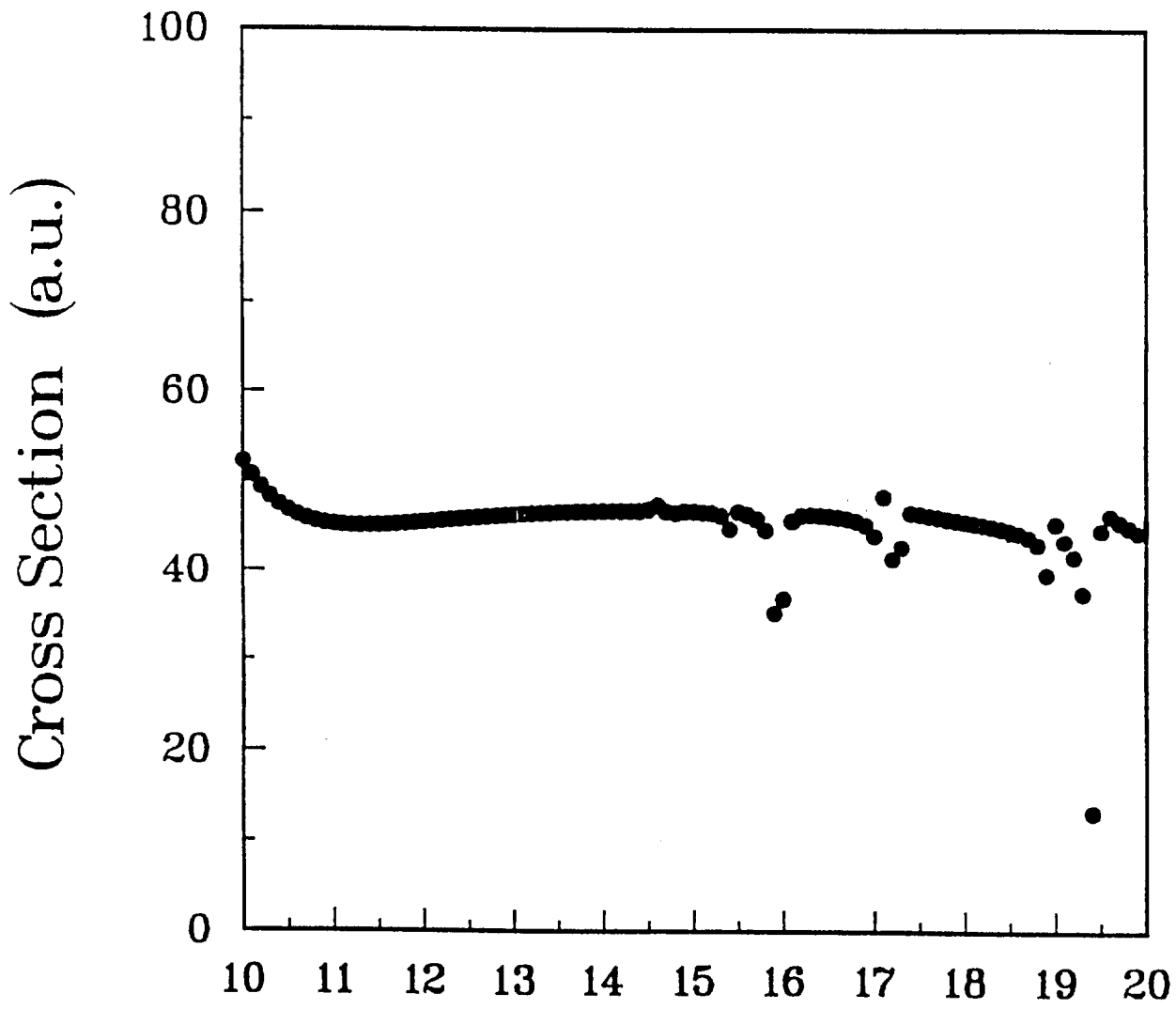
## Figure Captions

- Fig. 1a e-CO elastic scattering cross section in the static-exchange approximation versus  $a$  at 3.75 eV electron energy. This figure depicts all data points where the cross sections are within 5% of each other.
- Fig. 1b Same as Fig. 1a except all data points are included.
- Fig. 2a e-H<sub>2</sub> elastic scattering cross sections at 13 eV as a function of  $a$ . This figure depicts all data points from the 70-basis calculations where the cross sections are within 10% of each other. The dashed line denotes the average cross section over the data points.
- Fig. 2b Same as Fig. 2a for cross sections determined using the 64-basis.
- Fig. 3a e-H<sub>2</sub>  $X^1\Sigma_g^+ \rightarrow b^3\Sigma_u^+$  excitation cross sections at 13 eV as a function of  $a$ . This figure depicts all data points from the 70-basis calculations where the cross sections are within 10% of each other. The dashed line denotes the average cross section over the data points.
- Fig. 3b Same as Fig. 3a for cross sections determined using the 64-basis.
- Fig. 4 e-H<sub>2</sub>  $X^1\Sigma_g^+ \rightarrow b^3\Sigma_u^+$  excitation cross sections as a function of electron energy. The experimental data are from Hall and Andric (Ref. 45),  $\diamond$ ; Nishimura and Danjo (Ref. 46),  $\circ$ ; and Khakoo et al. (Ref. 47),  $\triangle$ .



a

*Fig. 1a*



a

Fig. 16

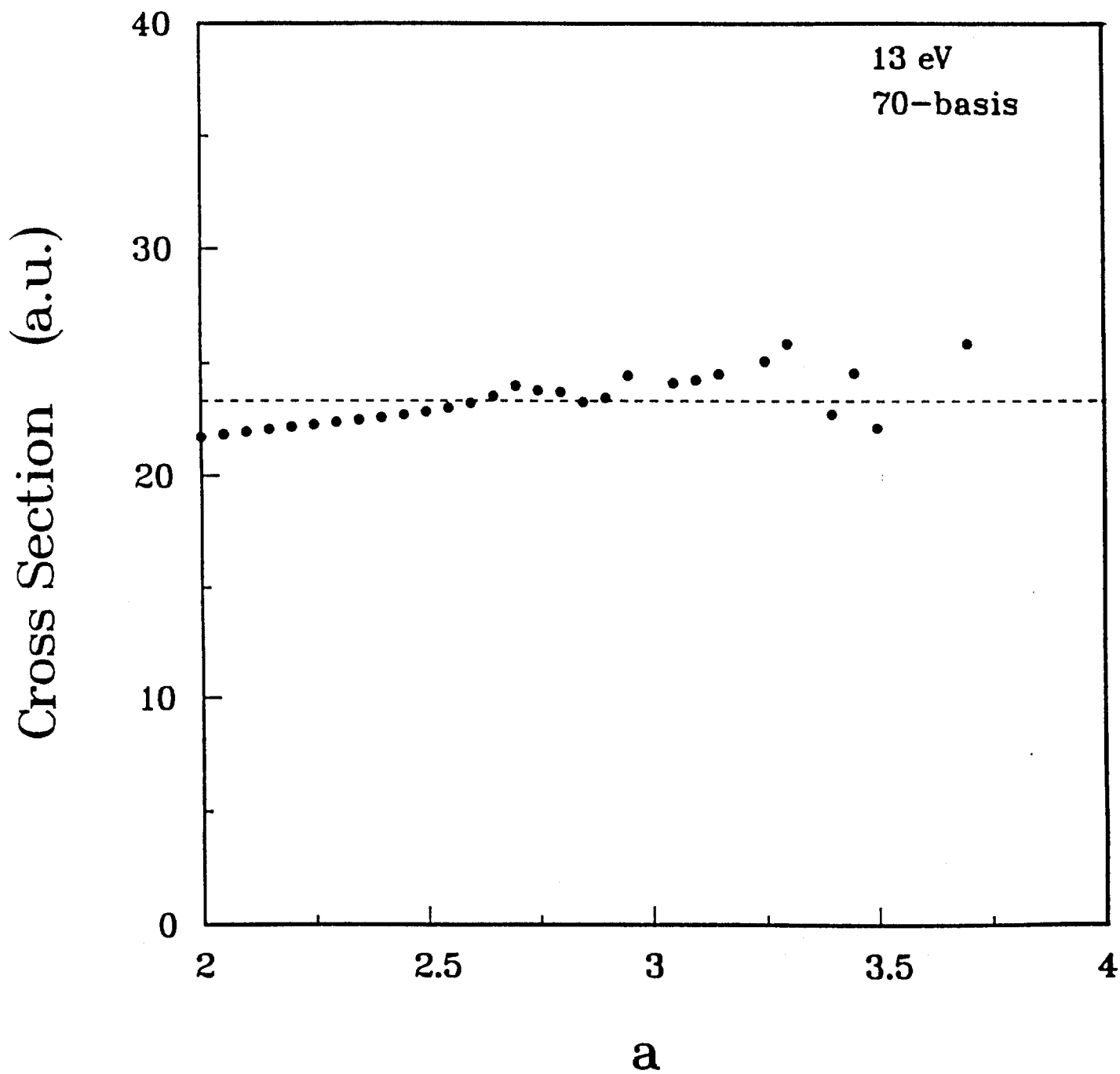


*Fig. 2a*

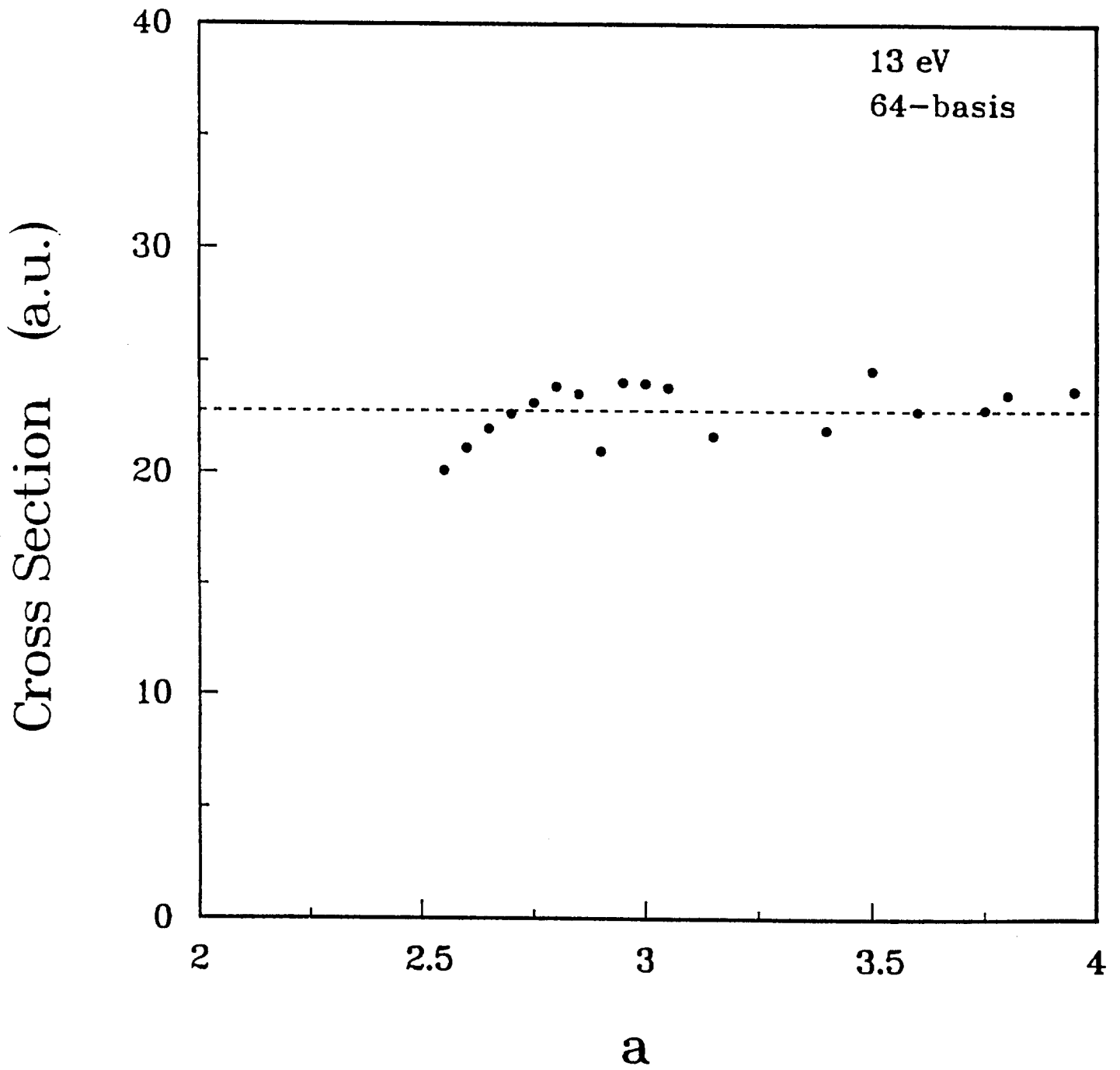


Fig. 26

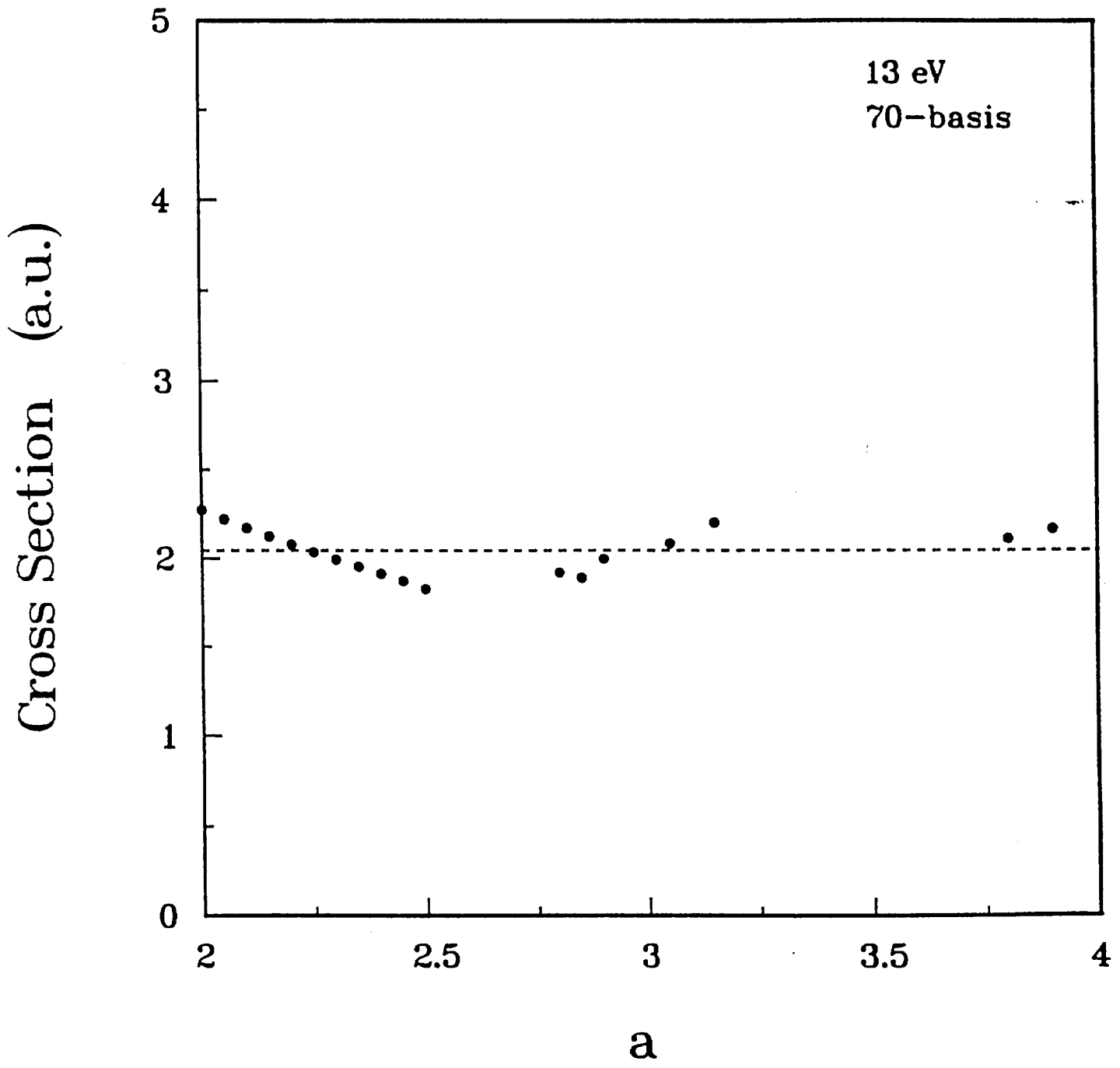


Fig. 3a

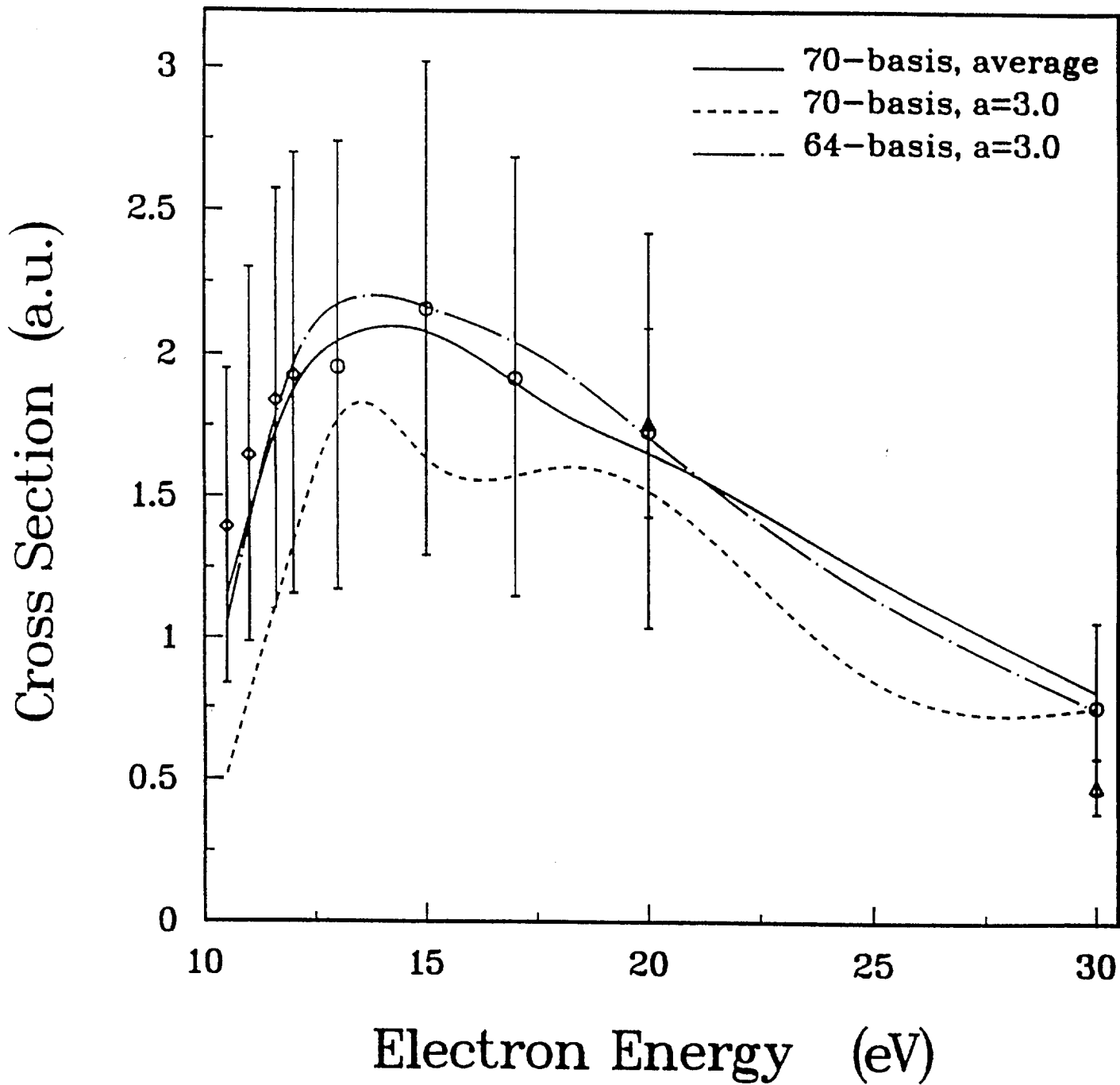


Fig. 4

# SCHRÖDINGER EQUATION MESH REQUIREMENTS IN THE FINITE DIFFERENCE DISCRETIZATION FOR NON-SPHERICAL POTENTIALS

by

**Charles A. Weatherford<sup>†</sup>**

Physics Department

and

Center for Nonlinear & Nonequilibrium Aeroscience

Florida A&M University

Tallahassee, FL 32307

U.S.A.

## ABSTRACT

The Schrödinger equation for the scattering of an electron by a hydrogen molecule is solved by converting it to a block-tri-diagonal matrix equation. The discrete mesh of points in the angular variable must be made more dense as the potential energy deviates from spherical symmetry to maintain a desirable level of accuracy. The present paper investigates the nature of this dependence, and the relative effect of third-order and fifth-order differentiation rules. It is found that the existence of one large element in the K-matrix sets a lower bound on the accuracy of all elements. This bound, and therefore the overall accuracy of the numerical approximation, can be substantially improved by the use of the higher-order rules.

<sup>†</sup>This work was supported by NASA contract NAGW-2930 and NCC 2-492. A grant of computer time from Florida State University is gratefully acknowledged.

Prepared for the 1993 DAMOP Conference in Reno, Nevada.

## 1. Introduction

Traditional electron scattering theory concerns the results of collisions between an electron and a target under the assumption that their interaction depends only on their separation, and is independent of their angular orientation. When the target is an atom, this assumption is justified, but when the target atoms are bound into molecules, the great simplifications afforded by the conservation of angular momentum are no longer available. A numerical analysis must therefore be introduced at an earlier stage in the solution of the problem.

The K-matrix is a concise and computationally simple means of presenting the results of a scattering calculation done by the method of partial differential equations. This work will investigate the relationship between the mesh size required in a finite-difference approximation to the K-matrix and the deviation of the scattering potential from spherical symmetry for various levels of accuracy. "Accuracy" is defined as the difference between the numerical approximation and a hypothetical continuum-limit K-matrix, which must be inferred from the behavior of the approximation.

The angular accuracy is roughly independent of the radial properties of the potential, so the numerical requirements of the polar-angle dependence can be investigated without a detailed model of the physical potential. The angular momentum quantum number  $l$  provides a convenient basis for calculating the K-matrix, but one which is not a basis of eigenvectors. In an eigenvector basis, the K-matrix would be diagonal, and the numerical convergence of the various elements would be unrelated, with the states of higher rotational energy requiring a finer mesh. Here, by contrast, the error in the numerical approximation is spread over all coupled states. In particular, if one element dominates the others, a small relative error in that element will imply a large relative error in the other elements. The convergence of the largest element is found to be excellent, with accuracy about  $10^{-3}$  using 29 points in the angular mesh. The convergence of the smaller elements is limited by this effectively constant bound. Convergence beyond this limit requires vastly larger meshes,

though a great improvement can be gained by the use of high-order differentiation rules. It is found that adding rules of fifth order in the mesh spacing requires little additional programming, and virtually no extra computer time.

## 2. The Method

The homonuclear diatomic molecule is the simplest system for which non-spherical terms contribute to the scattering potential, so it will serve as the physical anchor for an otherwise mathematical study. When the energy of the incident electron is between 1 and 10 electron volts, the non-spherical structure of the molecule is particularly important. In such a situation we use the axial symmetry of the molecule to reduce the Schrödinger equation to a two-dimensional partial differential equation. We assume for simplicity that the collision does not excite vibrational states of the molecule. Rotational excitations may be dealt with at the cross-section stage of the calculation in the usual adiabatic-nuclei manner [1].

The target molecule may be assumed to be oriented in a particular direction in space, so we use the axis of symmetry of the molecule as the z-axis of our coordinate system (Figure 1), and define a modified wave function  $u$  which is related to the true wave function  $\Phi$  for the projectile by

$$\Phi(r, \vartheta, \phi) = r^{-1}u(r, \vartheta) e^{im\phi}. \quad (1)$$

The equation for  $u$  in atomic units is

$$\frac{\partial^2 u}{\partial r^2} + r^{-2} \left\{ \cot \vartheta \frac{\partial u}{\partial \vartheta} + \frac{\partial u}{\partial \vartheta} \right\} + \left\{ p^2 - 2V(r, \vartheta) - \frac{m^2}{r^2 \sin^2 \vartheta} \right\} u = 0. \quad (2)$$

where  $V(r, \vartheta)$  is the scattering potential, and  $p$  is the momentum of the projectile. A finite

difference approximation to this equation is solved on the domain  $0 \leq r \leq R_{\max}$ ,  $0 \leq \vartheta \leq \pi/2$ . The outer limit  $R_{\max}$  is chosen to be sufficiently large that the scattered particle is effectively free at that distance. The range of  $\vartheta$  has been cut in half to take advantage of the symmetry of the molecule under reflections in the x-y plane.

The boundary condition at  $r=0$  requires that  $u=0$ . At  $\vartheta=0$ , there are two possibilities: if  $m$ , the z-component of the orbital angular momentum, is nonzero, then  $u=0$ ; otherwise  $\partial u/\partial \vartheta=0$ . At  $\vartheta=\pi/2$ , the parity of the system dictates either that  $u=0$  or  $\partial u/\partial \vartheta=0$ . At  $r=R_{\max}$ , we impose the requirement that the incoming electron be in a state of well-defined orbital angular momentum, so

$$u(R_{\max}, \vartheta) = P_{lm}(\cos \vartheta). \quad (3)$$

The parity of the associated Legendre function,  $(-1)^{l+m}$ , determines the choice of boundary condition at  $\vartheta=\pi/2$ . Though this parity is conserved by the scattered wave function, the value of  $l$  for the incident wave is not. Outgoing waves therefore contain a superposition of  $l$ ,  $l\pm 2$ ,  $l\pm 4$ , and so forth.

Once the wave function has been found, information about the scattering is extracted by matching it to the known asymptotic form

$$\Phi_{lm} = \sum_{\Gamma} [A_{\Gamma} j_{\Gamma}(pr) + B_{\Gamma} y_{\Gamma}(pr)] P_{\Gamma m}(\cos \vartheta), \quad (4)$$

where  $l$  and  $m$  are the index and order of the Legendre function used in the boundary condition at large  $r$ , and  $j$  and  $y$  are spherical Bessel functions. The coefficients  $A$  and  $B$  form matrices on the

space of allowed values of orbital angular momentum.

The orthogonality of the Legendre functions may be used to project out a particular value of  $l'$ . When this is done for two different large values of  $r$ , the linear independence of the Bessel functions allows extraction of the unknown coefficients  $A$  and  $B$ . This process must be done for each allowed value of  $l'$ ; then, the whole solution process repeated, allowing  $l$  to take on each permitted value. The result is two matrices describing the transformation of an angular momentum eigenstate into a scattered wave. In principle, the dimension of the matrices is infinite, but in practice the finite range of the non-spherical potentials provides a cutoff. For an  $H_2$  molecule, with a projectile energy below 10 eV, values of  $l$  less than 5 are all that are required. Hence, the matrices are at most  $3 \times 3$ . The  $K$ -matrix is defined by the equation

$$\Phi_{lm} = \sum_l [j_l(pr) + K_{ll'} y_l(pr)] P_l^m(\cos \vartheta), \quad (5)$$

so  $K = A^{-1}B$ , and the influence of the artificial imposition of an initial orbital state is removed. The diagonal elements of  $K$  are the tangents of the elastic phase shifts, and the off-diagonal elements describe the coupling of states of different orbital angular momentum by the potential.

### 3. The Potentials

The potential energy function  $V$  in equation (2) represents the electromagnetic interaction of the projectile with the target molecule, and is the source of the breaking of spherical symmetry. In principle, this interaction is highly complicated. A molecule is by no means a static, rigid body in the presence of an incoming electron, so a potential model is not strictly correct, but the practical usefulness of potentials in calculations is great enough to excuse the gross simplification of the scattering problem they imply. The potentials involved in scattering from hydrogen molecules are approximations to three effects: the static electric moments of the molecule; the polarization of the molecule by the electric field of the projectile; and the substitution of an electron from the molecule

for the projectile in the outgoing state, known as "exchange". Toy models have been adopted which mimic to some extent the radial structure of the physical potentials, and have angular properties which are expandable in the low-order Legendre polynomials of even parity.

Because the hydrogen molecule is composed of identical atoms, the lowest-order multipole field seen by the projectile is the quadrupole term

$$V_Q(r, \vartheta) = Q r^{-3} P_2(\cos \vartheta), \quad (6)$$

where  $Q=0.49$  in atomic units. This form is valid for values of  $r$  which are outside the molecule for all  $\vartheta$ . At shorter ranges, the quadrupole potential is cut off by the usual exponential term  $(1-\exp[-(r/a)^6])$  as a multiplier. The adjustable parameter  $a$  is set to 1, since no effort is made to fit experimental data. The static potential inside the molecule is represented by a Yukawa function of unit range and arbitrary strength, which is adjusted as necessary to give the correct order of magnitude for the K-matrix.

Polarization of the target is well known to include terms of both spherical and  $P_2$  character [1]. The form used here is

$$V_P(r, \vartheta) = r^{-4}(1-\exp[-r^6]) [a_0 + a_2 P_2(\cos \vartheta)]/2, \quad (7)$$

with  $a_0=5.5$ , and  $a_2=1.4$ .

The exchange potential is a crude form of the Free Electron Gas model. The basic idea here is that the electrons in the target may be approximated by a degenerate Fermi gas whose density varies with position [1]. The exchange potential is proportional to the Fermi momentum at any point in space, giving

$$V_x(r) = -(3/2\pi) [3\pi^2 \beta(r)]^{1/3}. \quad (8)$$

The electron density  $\beta(r)$  is approximated by a simple sum,

$$\beta(r, \vartheta) = (4\pi)^{-1} e^{-r} [1 + 1.3 P_2(\cos \vartheta)], \quad (9)$$

which has contours of constant density which resemble those of the sum of two hydrogen atoms separated by .7 angstroms. The resulting potential can be approximated by a linear combination of Legendre polynomials, which is

$$V_x(r, \vartheta) = -.8 e^{-r/3} [.97 + .43 P_2(\cos \vartheta) + .1 P_4(\cos \vartheta)]. \quad (10)$$

The "realistic" potential is a sum of these three terms.

The long-range quadrupole potential is the most important term in real scattering problems, but it does not vanish until a distance of 14 Bohr radii from the molecule's center is reached. This was determined *a posteriori*, by searching for a region in which the K-matrix does not depend on small changes in  $R_{\max}$ .) Such a long range requires a large number of radial points, and consequently a long running time for the computer code. Although the convergence properties of the angular approximation are roughly independent of the quality of the radial approximation, this independence is only valid when the radial mesh is on the order of magnitude of the mesh which gives decent radial convergence. Therefore, the quadrupole term is generally omitted from this work, in the interest of a more efficient use of computer time. The  $P_2$  terms in the polarization and exchange potentials are in any case expected to yield the same requirements on the angular mesh.

#### 4. Numerical Analysis

The usual discrete approximation to equation (2) is obtained by replacing the radial variable with a set of  $N_r$  points, and the angle with a set of  $N_\theta$  points. The wave function therefore becomes a set of (real) values which solve the equation [2]

$$\begin{aligned}
& h_r^{-2} [u_{i+1,j} - 2u_{i,j} + u_{i-1,j}] + \\
& r_i^{-2} [h_o^{-1} \cot \vartheta_j (u_{i,j+1} - u_{i,j}) + h_o^{-2} (u_{i,j+1} - 2u_{i,j} + u_{i,j-1})] + \\
& [p^2 - 2V_{i,j} - m^2 / r_i^2 \sin^2 \vartheta_j] u_{i,j} = 0. \quad (11)
\end{aligned}$$

Here,  $u_{ij}=u(r_i, \vartheta_j)$ , with  $0 < i \leq N_r$  and  $0 < j \leq N_o$ . The spacings between the radial and angular points are  $h_r$  and  $h_o$ , respectively. (The values of  $h_r$  and  $h_o$  may in principle depend on  $i$  and  $j$ .) Equation (11), together with the boundary conditions, gives a system of  $(N_r+2)(N_o+2)$  coupled linear equations for the  $u_{ij}$ , which may be solved by conventional matrix methods [3].

The choice of the points  $r_i$  and  $\vartheta_j$  presents an unavoidable conflict of interest. There are ways to improve the accuracy of a numerical solution of a differential equation by judicious choice of abscissae, just as there are ways to improve the numerical quadrature by which the elements of the K-matrix are projected out of the wave function. Unfortunately, the ways are mutually inconsistent. Numerical quadrature is optimized by choosing points so that successive errors alternate in sign, which is the worst possible choice of points for differentiation. Therefore, a compromise of equally-spaced abscissae will be used, and optimization achieved through higher-order integration and differentiation rules.

When the Schrödinger equation is solved on a two-dimensional lattice, the resulting matrix is block tridiagonal. This property, which makes the matrix easier to decompose into lower and upper triangular matrices, depends on one of the variables having a simple three-point derivative. The other may be as complicated as the problem demands. In this work, the radial accuracy is of secondary interest, so the  $\vartheta$ -derivative part of equation (11), which is in braces, will be explored with rules of greater accuracy (Table 25.2 in reference [4]).

For a point in the interior of the domain of approximation of  $\vartheta$ , labelled by "j", rules of order  $h_o^5$  are

$$\partial f / \partial \vartheta = (1/D_1) \{ 2f_{j-2} - 16f_{j-1} + 16f_{j+1} - 2f_{j+2} \}, \quad (12)$$

$$\partial^2 f / \partial \vartheta^2 = (1/D_2) \{ -f_{j-2} + 16f_{j-1} - 30f_j + 16f_{j+1} - 2f_{j+2} \}, \quad (13)$$

where  $D_1 = 24h_o$  and  $D_2 = 12h_o^2$ . (To simplify the formulae,  $u_{i,j}$  has been replaced by  $f_j$ .) For points next to the boundary, asymmetrical rules must be used:

$$\partial f / \partial \vartheta = (1/D_1) \{ -6f_{j-1} - 20f_j + 36f_{j+1} - 12f_{j+2} + 2f_{j+3} \}; \quad (14)$$

$$\partial^2 f / \partial \vartheta^2 = (1/D_2) \{ 11f_{j-1} - 20f_j + 6f_{j+1} + 4f_{j+2} - f_{j+3} \}. \quad (15)$$

These rules are used for points next to the boundary at  $\vartheta=0$ . Next to  $\vartheta=\pi/2$ , the subscript "j+3" is replaced by "j-3", "j+2" by "j-2" and so forth, and there is an overall minus sign in the first derivative.

At the boundary, if  $u=0$  is the boundary condition, then it goes directly into the matrix. If Neumann boundary conditions apply, the process is more involved. First, terms in the Schrödinger equation proportional to  $\partial f / \partial \vartheta$  are dropped. Then, equation (14) is used with  $j=0$  to get the relation

$$-6f_{-1} - 20f_0 + 36f_1 - 12f_2 + 2f_3 = 0 \quad (16)$$

which is solved for  $f_{-1}$ . This value is then used in equation (15) (with  $j=0$  again), to derive an expression for  $\partial^2 u / \partial \vartheta^2$  at  $J=0$  which is accurate to fifth order in  $h_o$ :

$$\partial^2 f / \partial \vartheta^2 = (1/D_2) \{ -(170/3)f_0 - 72f_1 - 18f_2 - (8/3)f_3 \}. \quad (17)$$

When Equation (17) is used in place of the second derivative term in (11), the result is an approximation which significantly improves the numerical accuracy, compared to the three-point rules. As a test, when a spherical potential is assumed, and the K-matrix calculated, the off-diagonal matrix elements should vanish. In fact, for a given number of  $\vartheta$  points, they are at most one fourth of those calculated with the three-point rules, and of order  $10^{-3}$  when the largest diagonal element is about 1.

## 5. Results

Convergence of the K-matrix is determined in two ways. The first takes advantage of the invariance of the K-matrix under time reversal to require that the K-matrix be symmetric. The second is that the value of an element of the K-matrix change with changes in the number of  $\vartheta$  points in a manner which points clearly to an asymptotic limit.

The matrices are not strictly symmetrical. When the scattering potential is spherical, the wave function should have the angular properties of the large-R boundary condition, all the way to the origin. This is true only when the boundary condition is  $l=0$ . When higher waves are used, each contains a contaminant of lower  $l$  values. This contamination decreases with each step in  $r$  away from the origin, reaching an eventual limit of about .002 times the amplitude of the correct wave. Therefore, any number less than .002 in the K-matrix is indistinguishable from zero. This seems to be an artifact of the solution algorithm, reducible only by improving the  $\vartheta$ -derivative rule.

(When a three-point rule is used, the corresponding limit is .008.)

The second criterion makes an accurate graphical depiction of the convergence difficult. The convergence of almost all elements is monotonic, so the choice of a specific limit is arbitrary, yet it has a great impact on the perceived quality of the convergence. For this reason, the first

derivative of  $K_{ll}$  with respect to  $N_0$  is plotted in Figures 2-7.

To best isolate the effects of various non-spherical potentials, the K-matrices used to produce figures 2-7 are derived from several potentials. First, a spherical Yukawa potential was used, then the same Yukawa potential multiplied by the Legendre polynomial  $P_2(\cos \vartheta)$ , then half of each. The length scale of the potential was 3, and its strength was set to -0.4. The momentum of the incoming particle was .8, corresponding to a kinetic energy of 8.7 eV. All these parameters were chosen to give significant K-matrix elements up to  $l=2$ . An exception is the  $P_2$  potential in Figure 5. The  $l=2$  element was very small, so its relative error was extremely large, and not indicative of the numerical properties of the algorithm. The fourth curve on the graphs is the "realistic" potential described above, with a Yukawa of unit range in place of the long-range quadrupole.

Figures 2 and 3 show the slope versus  $N_0$  of the K-matrix element for transitions between spherical waves. Figure 2 is for a three-point rule, and Figure 3 is for the five-point rules. The advantage of the five-point rule is most obvious at small numbers of theta points. As the mesh becomes finer, the relative advantage of the five-point rule diminishes, but it is still a factor of two better. Figures 4 and 5 are the same, for the D-wave to D-wave reaction.

Figures 6 and 7 are different. They show the difference between the  $l=0$  to 2 matrix element and the 2 to 0 element, and thus provide a test of time-reversal. The difference is normalized to the value of  $K_{02}$ , usually the smaller of the two. In judging the size of the relative error, it should be borne in mind that there is always a diagonal element of the K-matrix which dominates this term by an order of magnitude. The uncertainty in this dominant element is the primary source of this error. In this place, the five-point rule shows its particular virtue. The five-point rule shows a more symmetrical K-matrix with 11 points in the mesh than the three-point rule with 30.

## 6. Conclusion

The addition of five-point approximations to the angular derivatives requires only minor changes in the computer code for solving partial differential equations. It preserves the block-tridiagonal character of the equivalent linear system, so it requires no extra running time, and it yields significant improvement in the accuracy of the numerical solution.

The chief drawback of the partial-differential-equation method for non-spherical scattering problems is that the coupling between states makes the relative error in the small elements of the K-matrix large, since it is a small fraction of a large number. The largest element of the K-matrix thus creates a "floor", a lower bound on the possible error in the other elements.

The contamination of the wave function by lower partial waves than the input boundary condition is the largest single source of error. It is an artifact of the  $u=0$  boundary condition at the origin. The natural tendency of this algorithm is to assume the smoothest possible wave function near  $r=0$ , and it takes several steps away from the boundary before the large- $r$  boundary condition can assert its dominance. A more sophisticated treatment of the radial derivatives might well be rewarded by a reduction of this defect.

Though this work has confined itself to the angular behavior of the wave function, the great improvements afforded by the higher-order approximations to the derivatives might have counterparts in the radial direction. This would destroy the tridiagonality of the matrix, but in applications where the size of the computer's memory is less of a constraint than the cost of processor time, it may be worthwhile.

### References

- [1] N.F. Lane, Rev. Mod. Phys. **52**, 29 (1980).
- [2] A. Temkin, C.A. Weatherford and E.C. Sullivan, in 1989 ICPEAC Proceedings. (?)
- [3] B. Carnahan, H.A. Luther and J.O. Wilkes, Applied Numerical Methods. NY: John Wiley and Sons, 1969.
- [4] M. Abramowitz and I. Stegun, Handbook of Mathematical Functions. NY: Dover Publications, 1970.

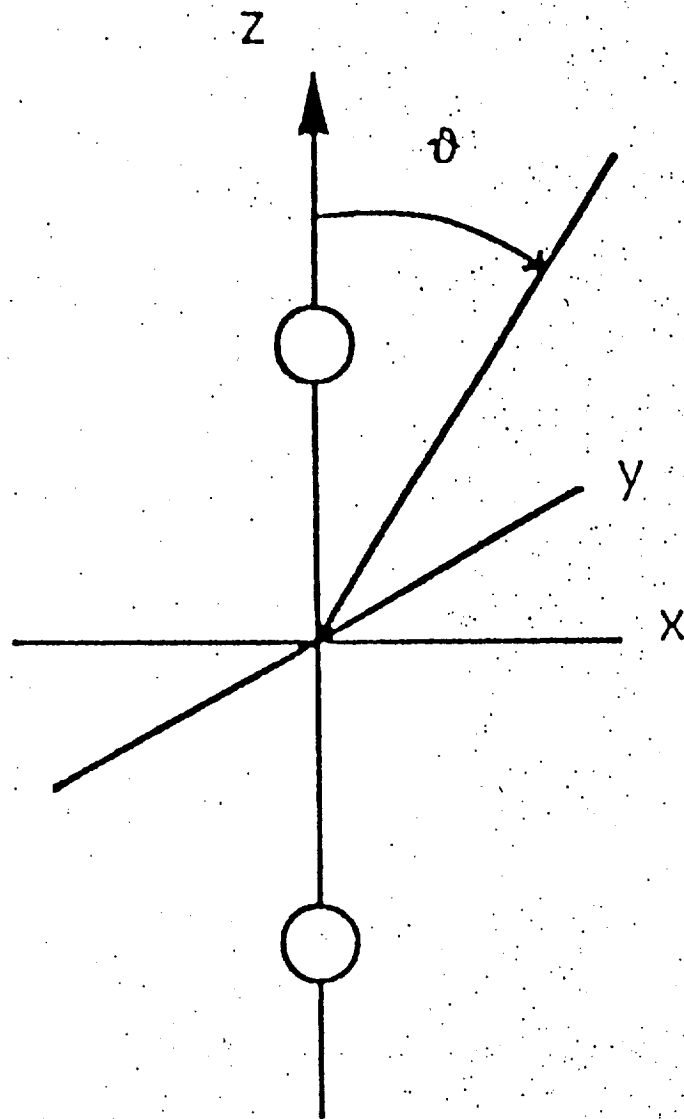


Figure 1. The coordinate system for scattering from a diatomic molecule.

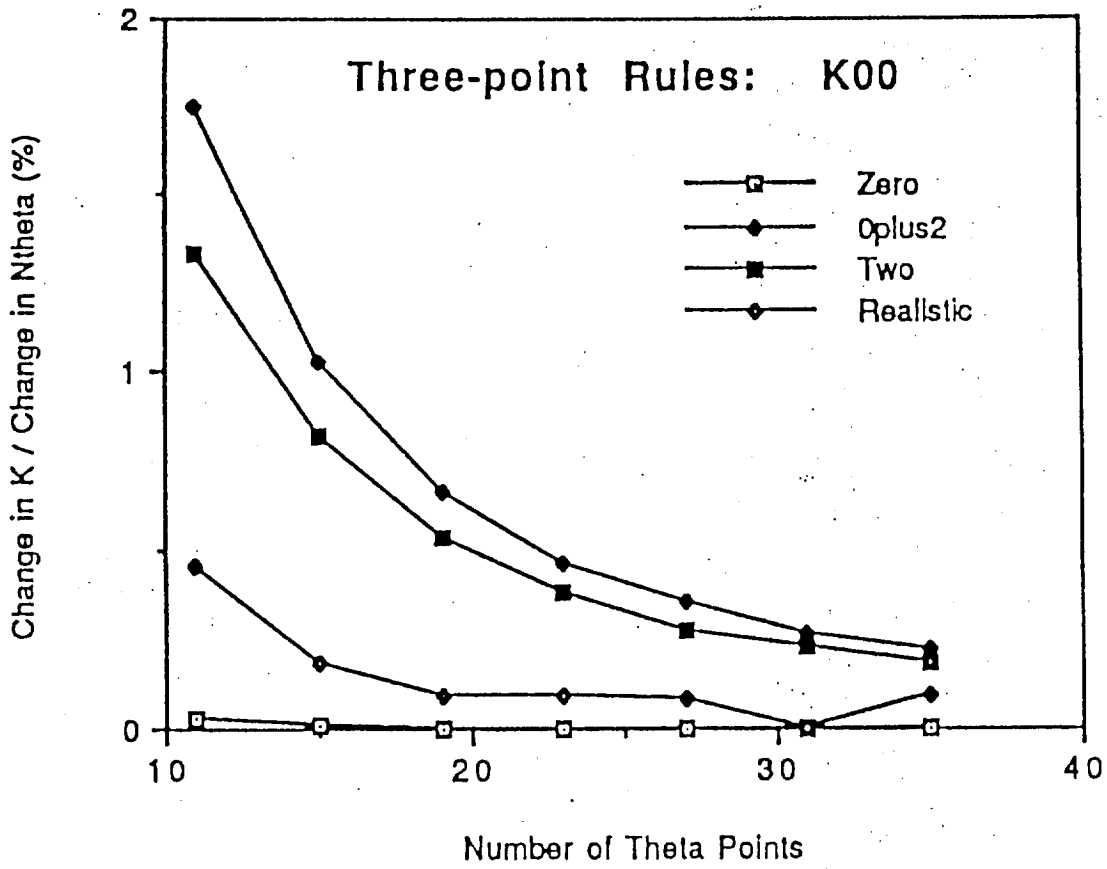


Figure 2. The relative change in the K-matrix element for S-wave to S-wave transitions, calculated using three-point derivative rules.

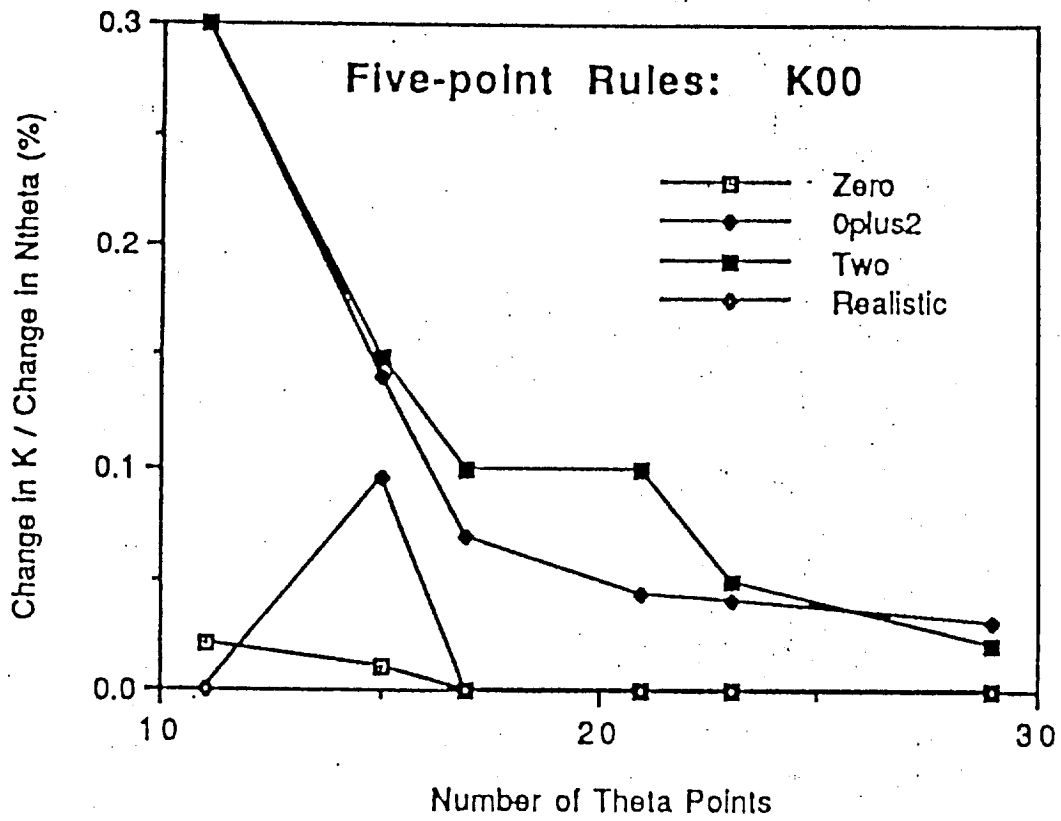


Figure 3. Same as Figure 2, but with five-point rules.

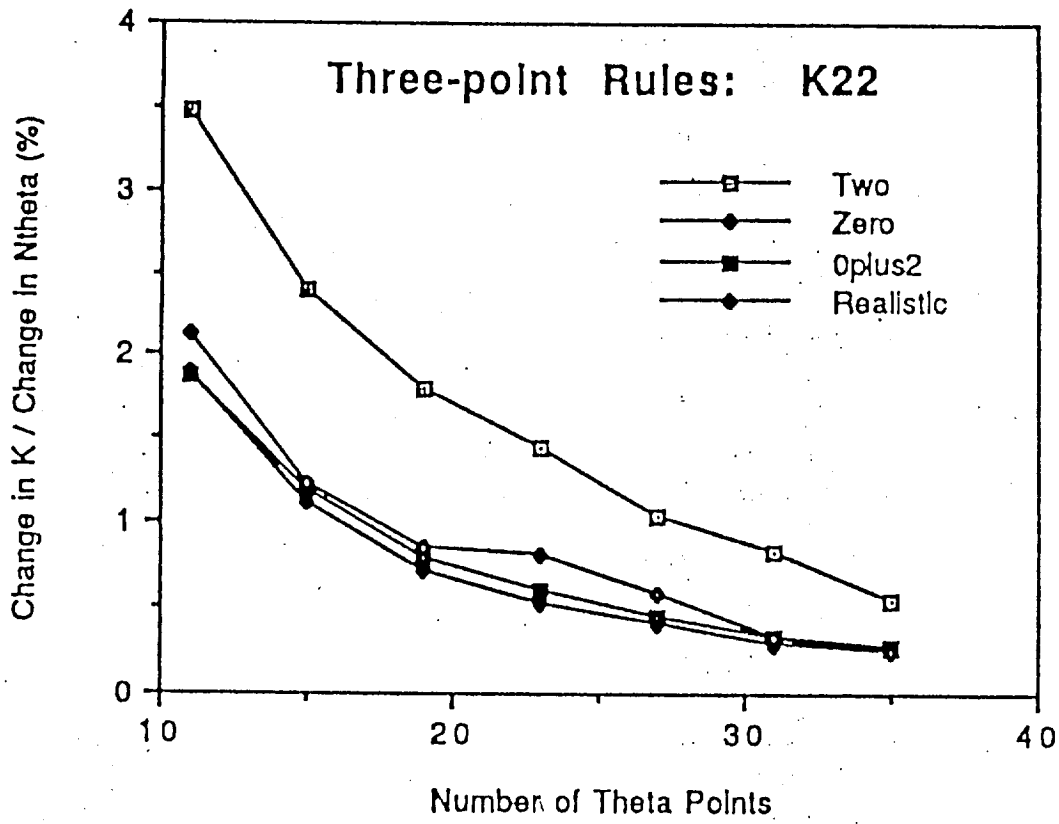


Figure 4. The relative change in the K-matrix element for D-wave to D-wave transitions, calculated using three-point derivative rules.

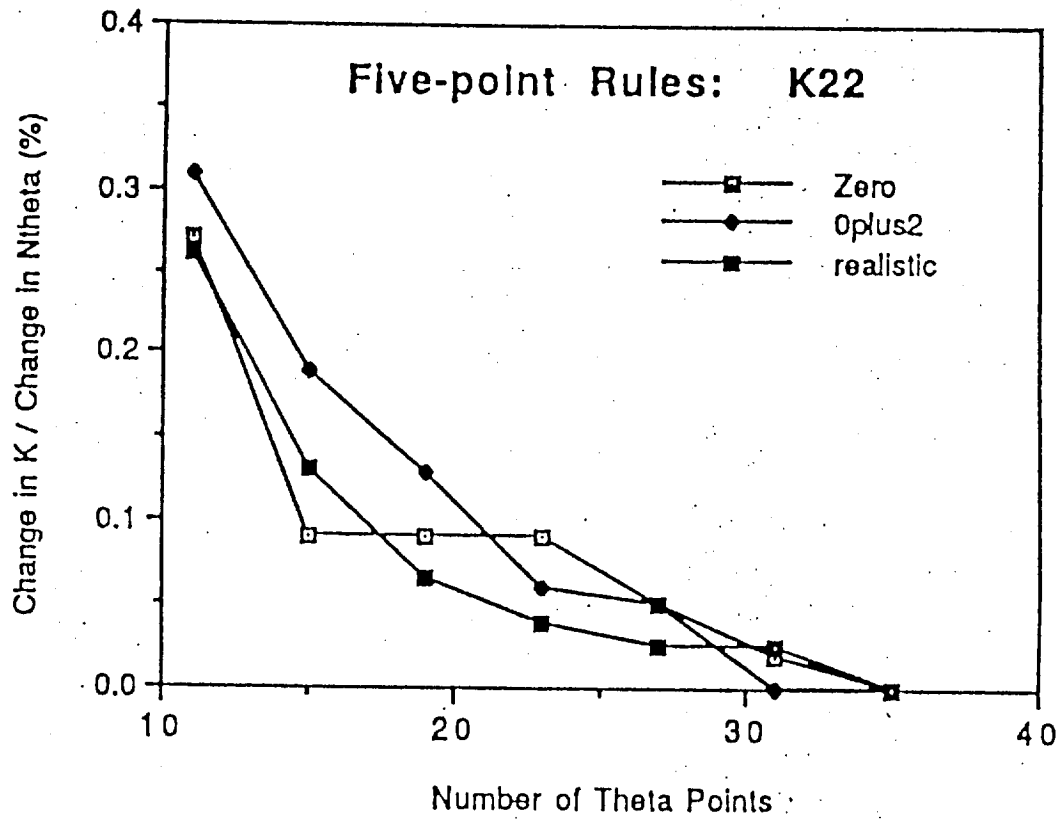


Figure 5. Same as Figure 4, but with five-point rules.

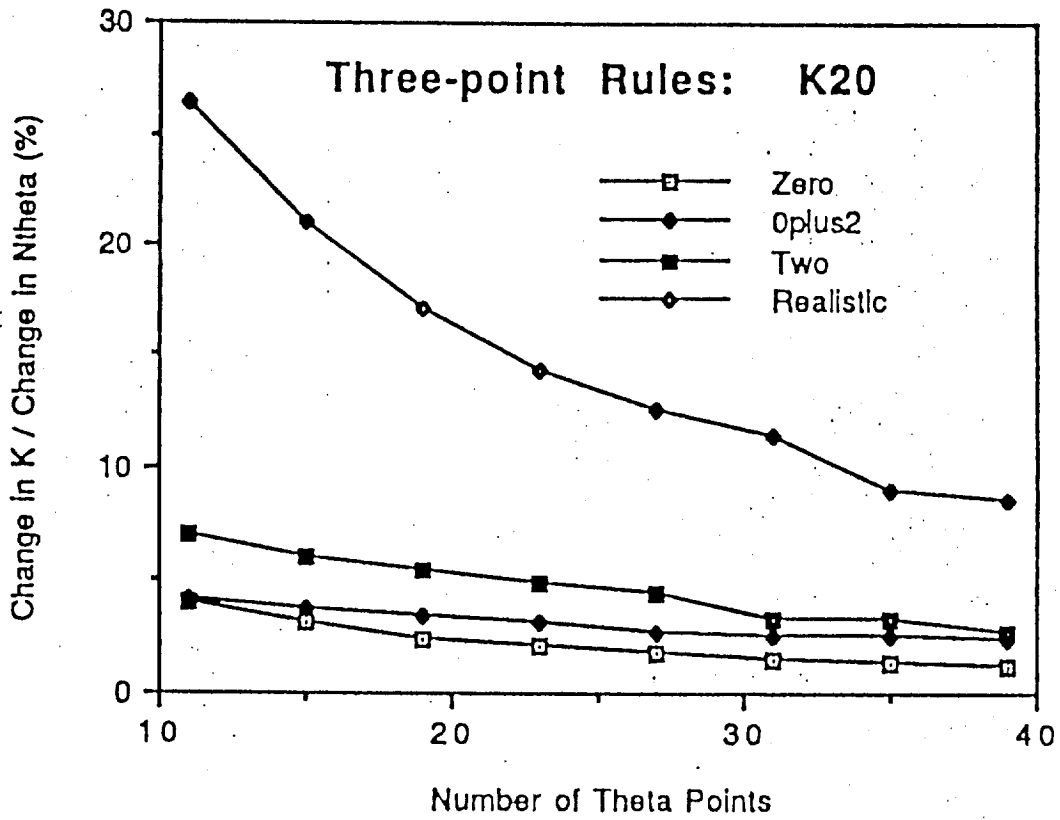


Figure 6. The relative change in the K-matrix element transitions between S- and D-waves, calculated using three-point derivative rules.

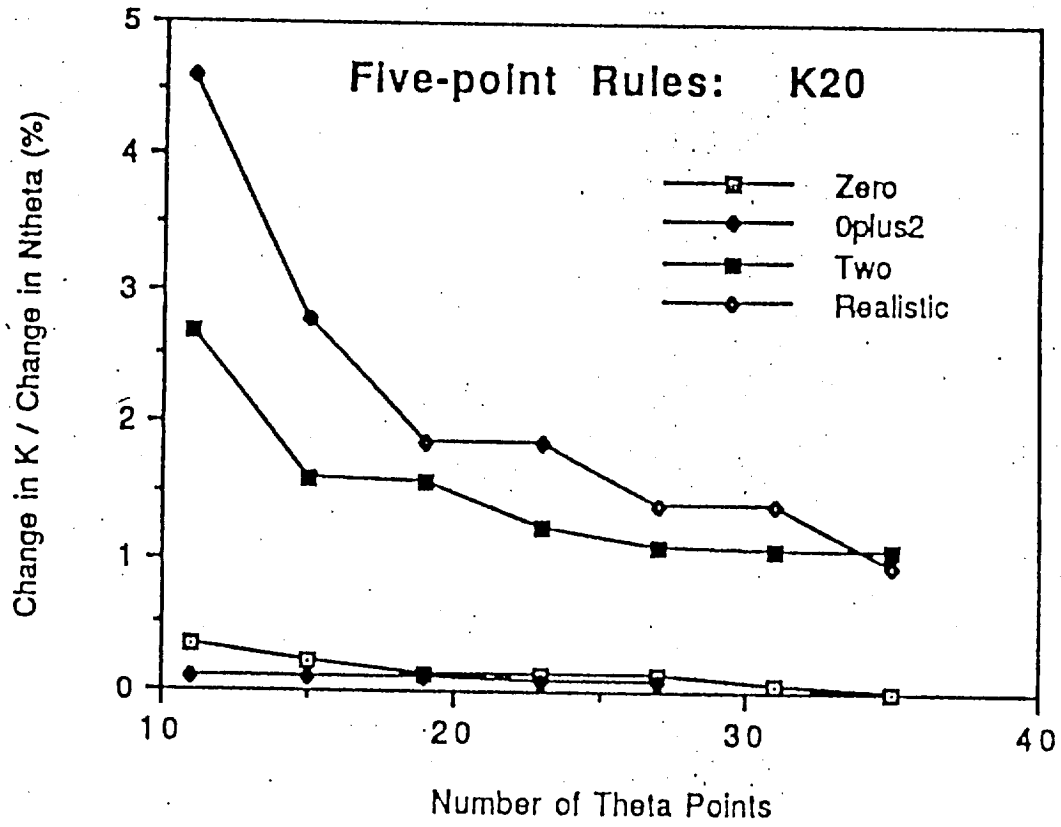


Figure 7. Same as Figure 6, but with five-point rules.

Figure 8: Three-point rules

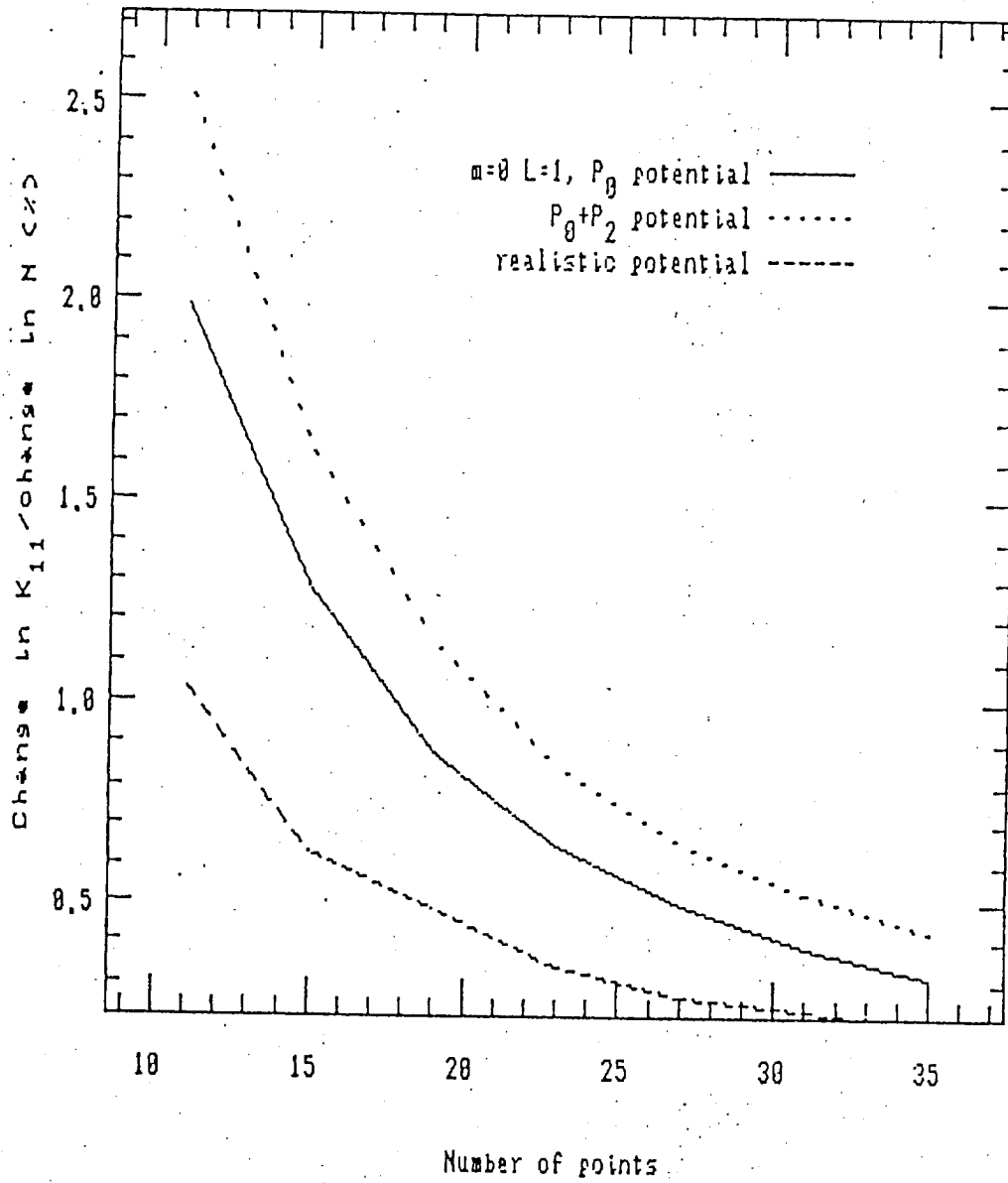


Figure 3: Five-point rules

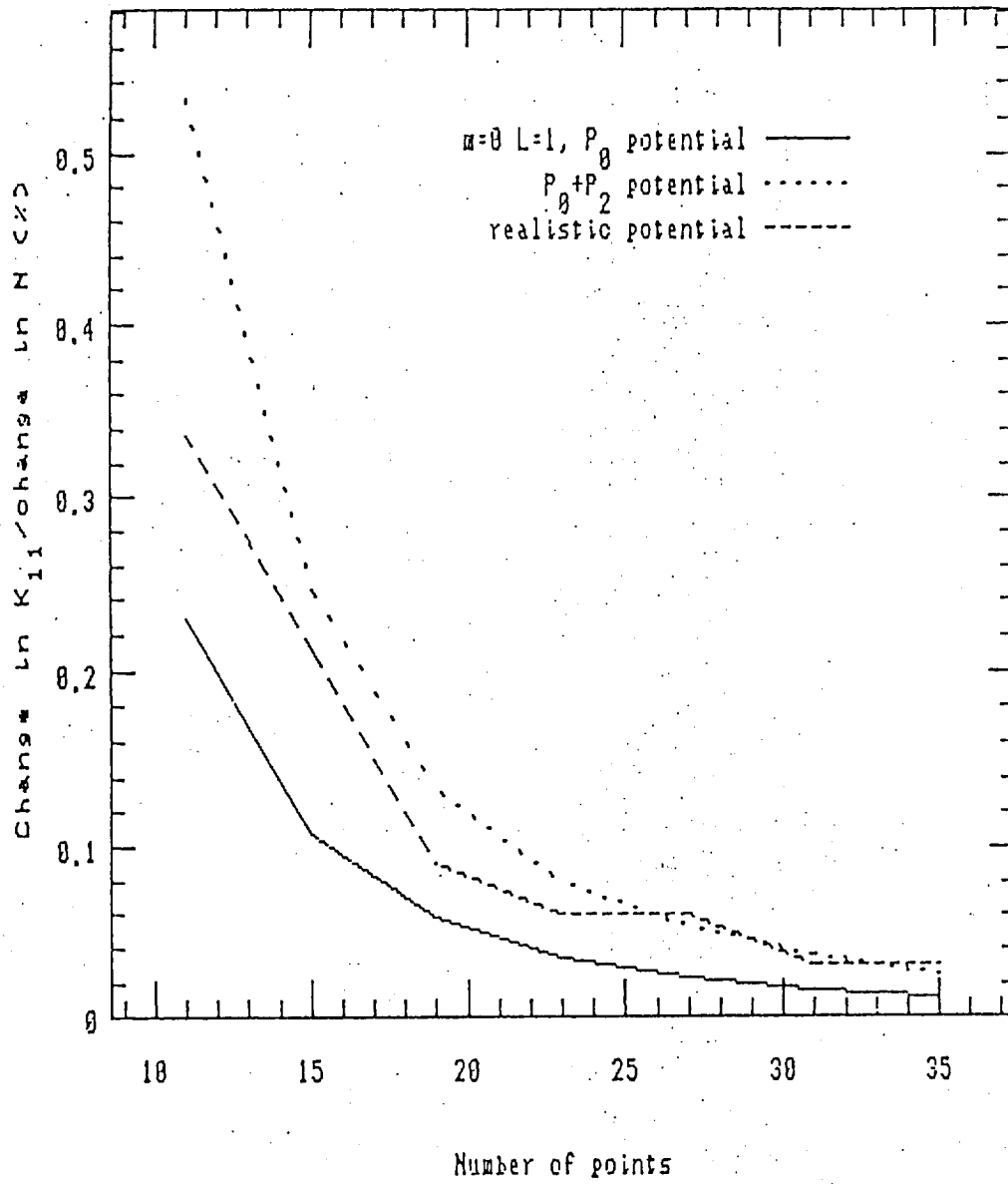


Figure 10: Three-point rules

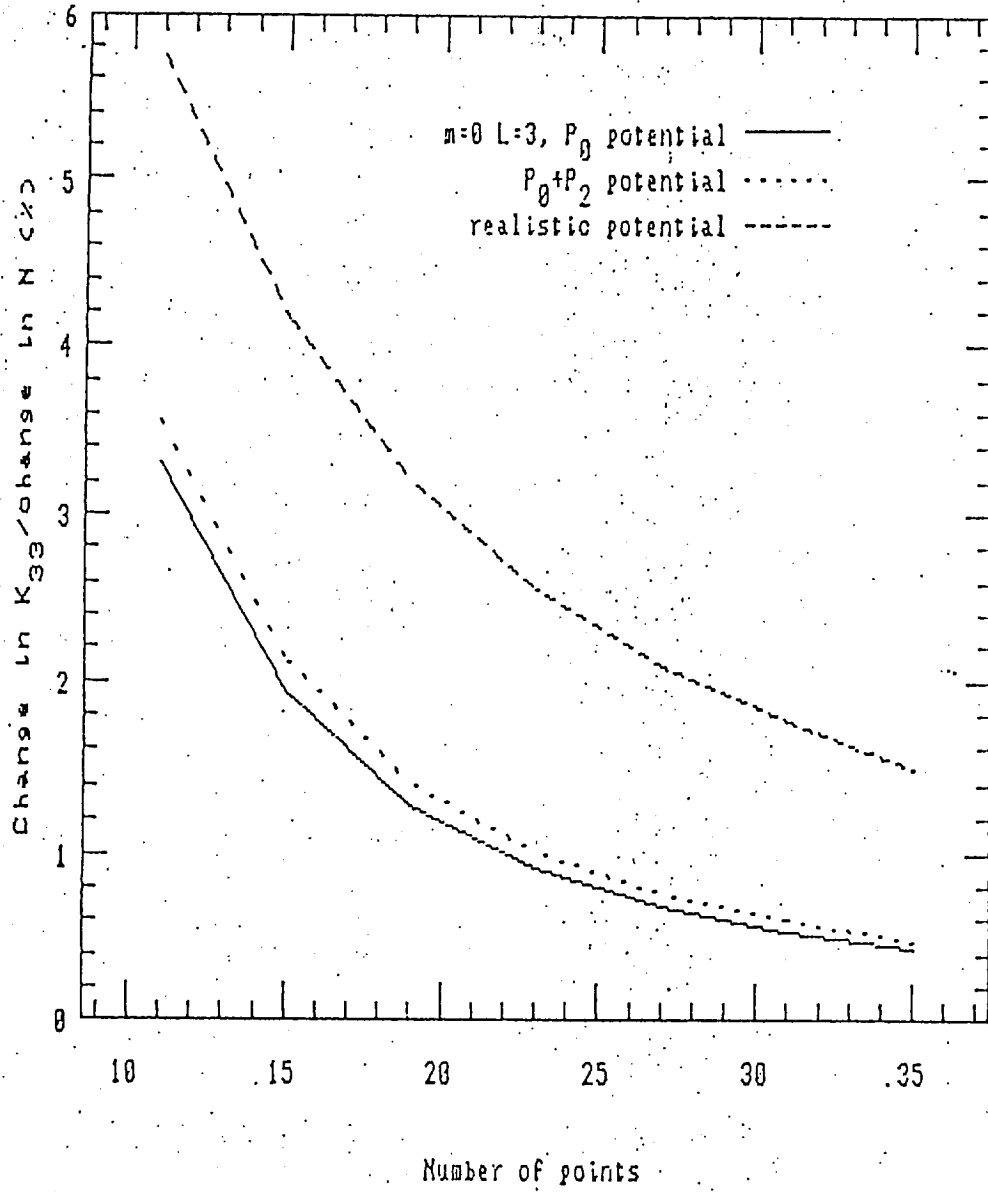


Figure 11: Five-point rules

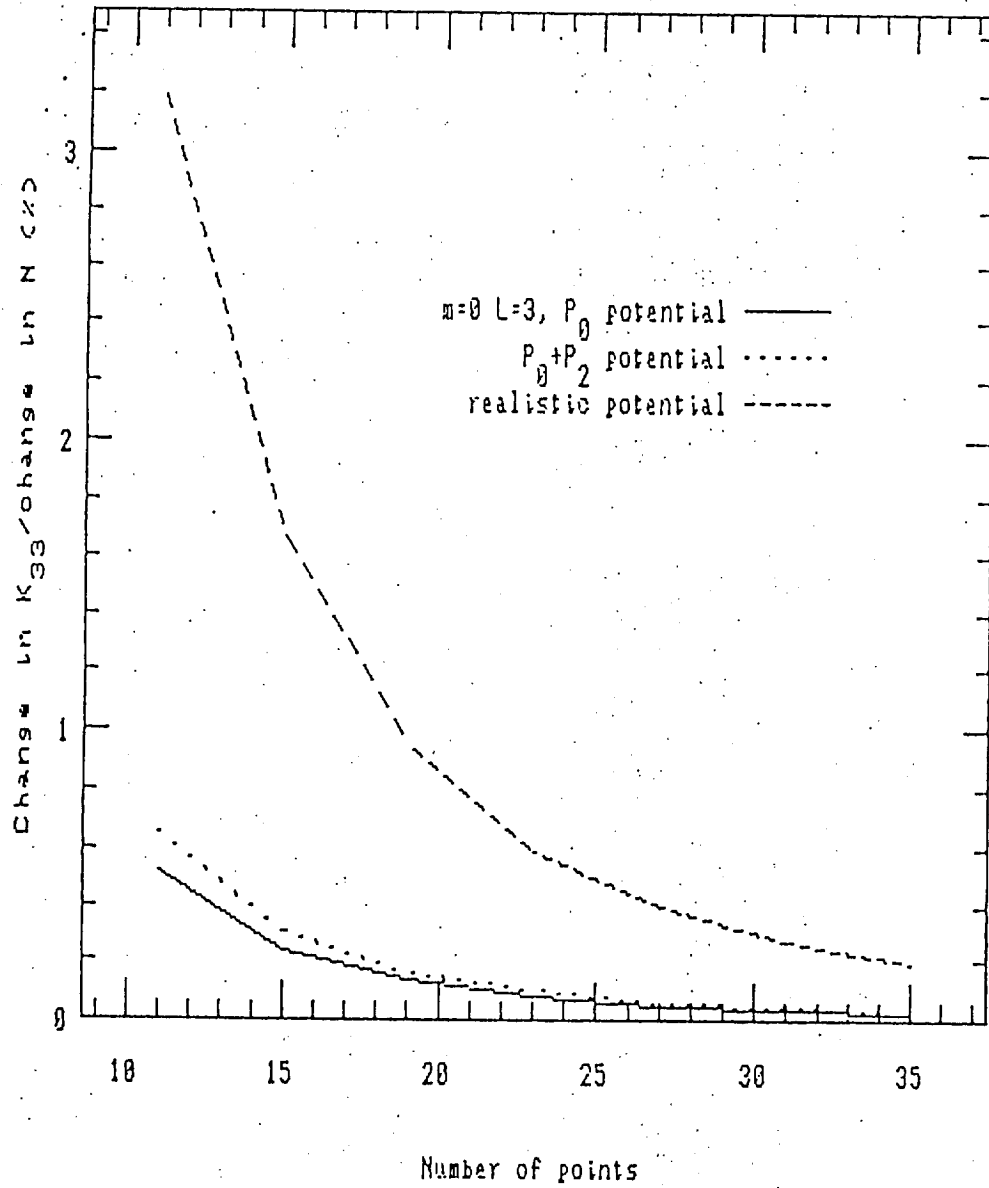


Figure 12: Three-point rules

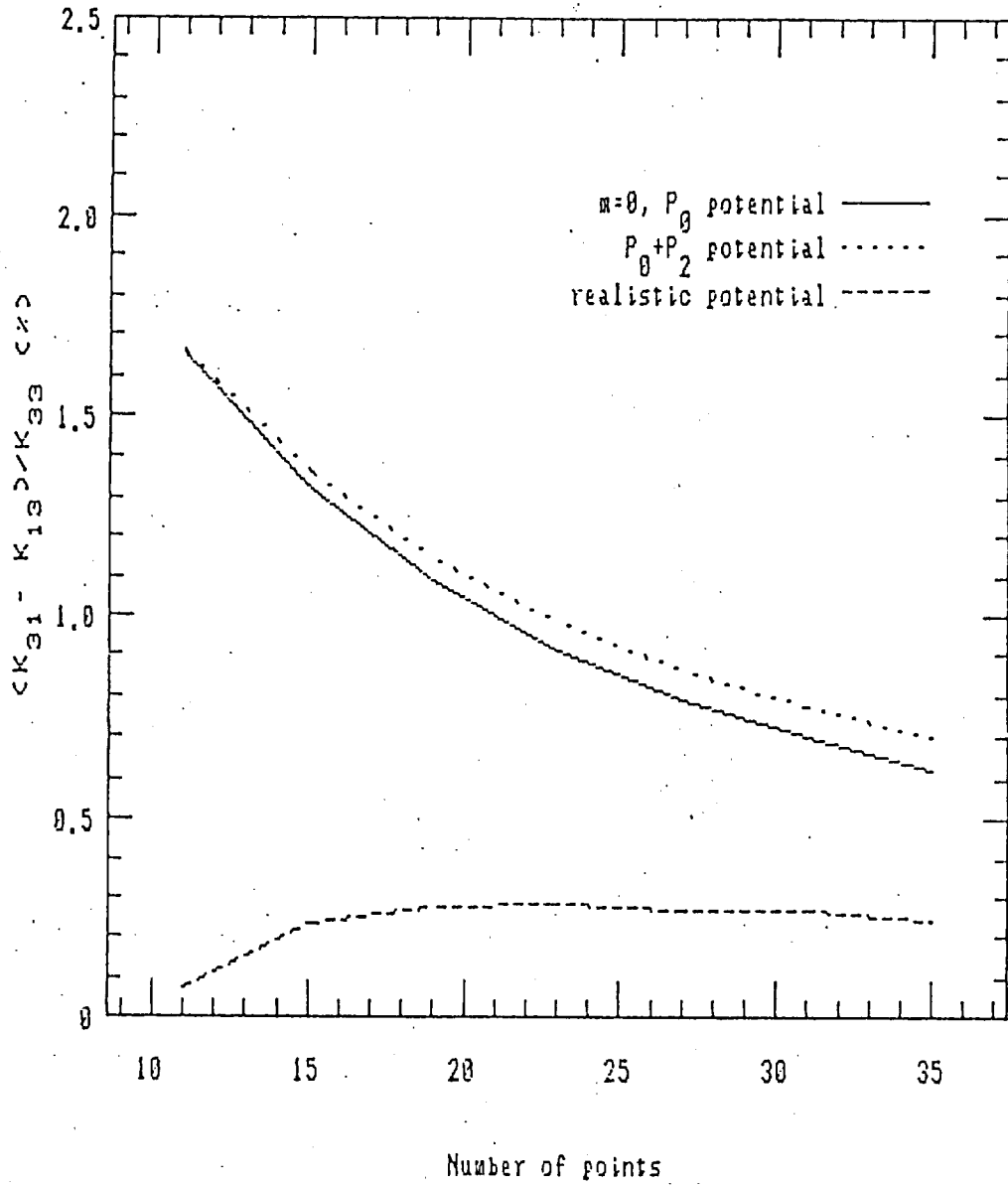
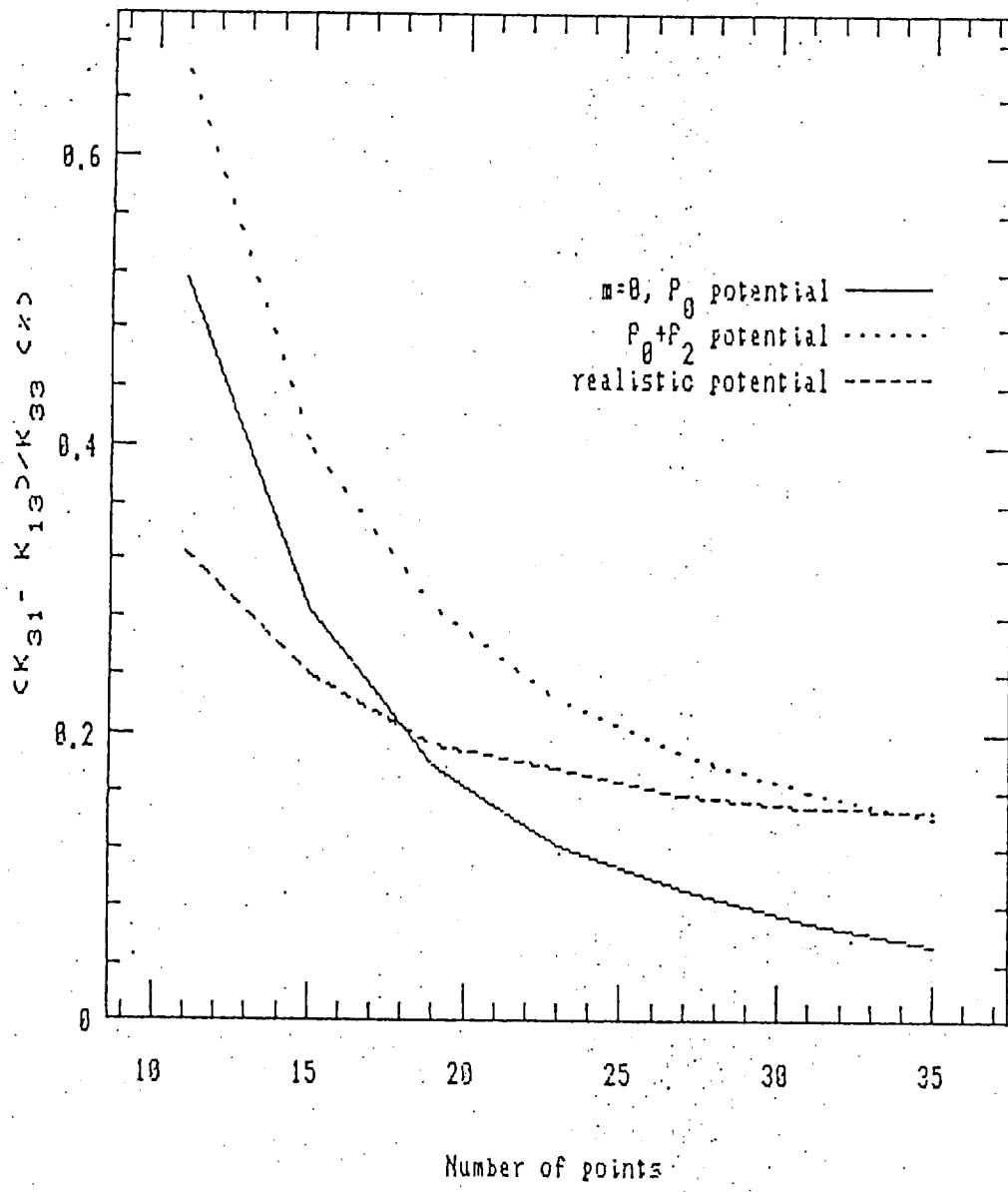


Figure 13: Five-point rules



# Completion of hybrid theory calculation of the $\pi_g$ resonance in electron- $N_2$ scattering

C. A. Weatherford<sup>(\*)</sup> and A. Temkin<sup>(+)</sup>

(\*) Department of Physics  
and  
Center for Nonlinear & Nonequilibrium Aeroscience  
Florida A&M University  
Tallahassee, FL 32307

(+) Laboratory for Astronomy and Solar Physics  
Goddard Space Flight Center  
NASA, Greenbelt, MD 20771

## Abstract

A calculation of e- $N_2$  scattering in the vicinity of the 2.4 eV ( $\Pi_g$ ) resonance has been completed. The main element of the calculation is a 15 term vibrational close coupling expansion, reduced to coupled two-dimensional (2d) partial differential equations (pde's), and solved using the noniterative pde technique. The potential consists of static, exchange, and polarization parts; each part has been (previously) derived in a manner appropriate to its importance in the scattering equation. Results for the absolute total cross section, both in magnitude and shape of the substructure in the resonance region ( $1.5 < k^2 < 3.0\text{eV}$ ), are in excellent accord with experiment. Angular distributions are also calculated and found to vary significantly in shape in the immediate vicinity of the center of the resonance ( $2.05 < k^2 < 2.15\text{eV}$ ), indicating the need for differential measurements at a finer grid in energy, and therefore, requiring even better energy resolution. Comparison with other calculations and discussion of some theoretical aspects are also included.

PACS 34.80.Gs, 34.80.Bm

This paper was prepared for submittal to the Physical Review A.

## I. INTRODUCTION

The purpose of this paper is to report a calculation of electron scattering from molecular nitrogen ( $e\text{-N}_2$ ) using the noniterative partial differential equation technique.<sup>1</sup> This calculation is confined to the energy region around the 2.4 eV resonance; it consists of a 15-state vibrational close coupling expansion for the resonant ( $\Pi_g$ ) partial wave combined with fixed-(plus adiabatic-)nuclei amplitudes for the other (contributing) partial waves. The underlying method is the hybrid theory.<sup>2</sup> We shall concentrate on the angular distributions for the lower vibrational states ( $v = 0, 1, 2$ ), showing that their shapes change very rapidly from one energy to the next as one traverses the energy region in the center of the resonance. Thus, despite the fact that several differential scattering experiments have been reported (to be discussed below), they do not have the energy resolution, nor have they attempted to explore the variation in the angular distributions in this narrow energy region in detail. It is one of our aims to motivate such experimental investigations.

Several important developments in our calculations have been made since the introduction of the hybrid theory<sup>2</sup>, which we have reported piecemeal since then. Briefly, the most salient of them are: the noniterative technique itself<sup>1</sup>, the reduction of the scattering equation to 2d form, which was first outlined in Ref. 3, in addition to which—it turns out—the 2d technique could also be applied to the derivation of the polarization potential<sup>4</sup>, as well as to a method for exactly including exchange in the static-exchange approximation.<sup>5</sup> And finally, the direct (i.e. non-exchange) static potential could be calculated<sup>6</sup> using a much better (MCSCF) approximation of the  $\text{N}_2$  ground state than the SCF approximation, used originally.<sup>2-5</sup> Some interim results using a 10 state vibrational expansion were reported in Ref. 7.

## II. THEORETICAL ASPECTS

We start with an antisymmetrized ansatz for the total wavefunction of the  $e\text{-N}_2$  system<sup>2,7</sup>:

$$\Psi^{(m)} = \sum_{i=1}^{15} (-1)^{p_i} F^{(m)}(x_i; R) \Phi_{\text{N}_2}(x^{(i)}; R) \quad (2.1)$$

Here  $x_i$  are the coordinates (space and spin) of the  $i^{\text{th}}$  electron and  $x^{(i)}$  is the collection of coordinates of the remaining (fourteen) electrons. The factor  $(-1)^{p_i}$  is the parity of a cyclic permutation ( $\hat{P}_i$ ) of the sequence  $1, 2, \dots, 15$ , thus making  $\Psi^{(m)}$  completely antisymmetric.

We first summarize the analysis, mostly of Ref. 5, whereby the basic integro-pde is

derived. (Note, however that we are here using Rydberg units as opposed to atomic units, used in Refs. [5,6]). Insertion of Eq. 2.1 into the Schrödinger equation, and premultiplication by the target ground state,  $\Phi_{N_2}$ , yields the static exchange approximation. We first consider the ground state ( $\Sigma_g^+$ ) to be represented by a single determinant (i.e. SCF approximation):

$$\Phi_{N_2} = \det(1\sigma_g^2 2\sigma_g^2 1\sigma_u^2 2\sigma_u^2 3\sigma_u^2 1\pi_{zu}^2 1\pi_{yu}^2; \Sigma_g^+) \quad (2.2)$$

Labelling the different orbitals  $\phi_\alpha$  [ $\alpha : 1\sigma_g, \dots, 1\pi_{yu}$ ], we recognize that each  $\phi_\alpha$  is an explicit function of the coordinates of a single electron and an implicit function of the internuclear separation  $R$ :

$$\phi_\alpha = \phi_\alpha(\vec{r}_1, \dots; R) \zeta_\alpha(\text{spin}) \quad (2.3)$$

When one includes the  $R$  dependence of  $\phi_\alpha$  and  $F^{(m)}$ , one derives<sup>7</sup> a 3d pde for  $F^{(m)}$ :

$$[-\nabla^2 + H_{vib}(R) + V(\vec{r}; R) - E_{sc}] F^{(m)}(\vec{r}; R) = 2 \sum_{\alpha=1}^7 W_\alpha^{(m)}(\vec{r}; R) \phi_\alpha(\vec{r}; R), \quad (2.4)$$

where  $V(\vec{r}; R)$  is (to begin with) the static potential between the scattered electron and the target ( $N_2$ ):

$$V_{static}(\vec{r}; R) = \langle \Phi_{N_2} | V_{e-mol} | \Phi_{N_2} \rangle \quad (2.5)$$

and  $W_\alpha$  are the (static) exchange kernels

$$W_\alpha^{(m)}(\vec{r}; R) = \int d^3 r' \phi_\alpha^*(\vec{r}'; R) \frac{2}{|\vec{r} - \vec{r}'|} F^{(m)}(\vec{r}'; R) \quad (2.6)$$

The energy appearing in Eqs. 2.4 and 2.5 is

$$E_{sc} = k_v^2 + \epsilon_v, \quad (2.7)$$

and  $H_{vib}(R)$  is the vibrational part of the target Hamiltonian from whose internuclear potential, vibrational wave functions ( $\chi_v$ ) and energies ( $\epsilon_v$ ) are evaluated. (In this calculation, the latter are obtained numerically from the MCSCF potential energy curve reported in Ref. 6.

For the static potential (2.5), we use an MCSCF approximation<sup>6</sup> of  $\Phi_{N_2}$ . An MCSCF wave function is a sum of determinants, whereas the right hand side (i.e. the exchange part) of the scattering Eq. 2.4 assumes that  $\Phi_{N_2}$  is a single determinant (i.e. SCF approximation). Thus (2.4) constitutes an admittedly unbalanced approximation, which

nevertheless seemed well justified<sup>6,7</sup> because (a) the exchange terms usually have a quantitatively smaller effect than the direct terms, and (b) when written as in (2.4), the exchange terms can be rigorously reduced to a coupled set of ordinary (i.e. non-integral) pde's.<sup>6</sup> This comes about by expanding  $F^{(m)}$  and  $W_\alpha^{(m)}$  in vibrational states  $\chi_\nu$  of  $N_2$

$$\begin{aligned} F^{(m)}(\vec{r}; R) &= \sum_{\nu=0}^{N_\nu} F_\nu^{(m)}(\vec{r}) \chi_\nu(R) \\ W_\alpha^{(m)}(\vec{r}; R) &= \sum_{\nu=0}^{N_\nu} W_\nu^{(m,\alpha)}(\vec{r}) \chi_\nu(R) \end{aligned} \quad (2.8)$$

and, using the well known property of the Coulomb potential as the Green's function of the kinetic energy,

$$\nabla^2 \left( \frac{1}{|\vec{r} - \vec{r}'|} \right) = -4\pi \delta(\vec{r}' - \vec{r}), \quad (2.9)$$

allows the scattering equation (2.4) to be reduced to coupled, but nonintegral pde's<sup>7</sup>:

$$\begin{aligned} [\nabla^2 + k_\nu^2] F_\nu^{(m)}(\vec{r}) &= \sum_{\nu'=0}^{N_\nu} \left[ V_{\nu\nu'}(\vec{r}) F_{\nu'}^{(m)}(\vec{r}) - \sum_{\alpha=1}^7 \phi_{\nu\nu'}^{(\alpha)}(\vec{r}) W_{\nu'}^{(m,\alpha)}(\vec{r}) \right], \\ \nabla^2 W_\nu^{(m,\alpha)}(\vec{r}) &= -4\pi \sum_{\nu'=0}^{N_\nu} \phi_{\nu\nu'}^{(\alpha)}(\vec{r}) F_{\nu'}^{(m)}(\vec{r}). \end{aligned} \quad (2.10)$$

The double indexed quantities in (2.10) are vibrational matrix elements of the unsubscripted quantities. Thus the matrix elements in Eqs. 2.10 are given by the following expressions:

$$\begin{aligned} V_{\nu\nu'}(\vec{r}) &= \langle \chi_\nu(R) | V(\vec{r}; R) | \chi_{\nu'}(R) \rangle, \\ \phi_{\nu\nu'}^{(\alpha)}(\vec{r}) &= \langle \chi_\nu(R) | \phi_\alpha(\vec{r}; R) | \chi_{\nu'}(R) \rangle, \\ W_\nu^{(m,\alpha)}(\vec{r}) &= \sum_{\nu'=0}^{N_\nu} \langle \phi_{\nu\nu'}^{(\alpha)}(\vec{r}') | \frac{2}{|\vec{r} - \vec{r}'|} | F_{\nu'}^{(m)}(\vec{r}') \rangle. \end{aligned} \quad (2.11)$$

Eqs. 2.10 can be further reduced to 2d pde's by exploiting the cylindrical symmetry of the various functions. As derived in Ref. 5, they take the form

$$\begin{aligned} [\Delta(m) + k_\nu^2] f_\nu^{(m)}(\underline{z}) &= \sum_{\nu'=0}^{N_\nu} \left[ V_{\nu\nu'}(\underline{z}') f_{\nu'}^{(m)}(\underline{z}) - \frac{1}{r} \sum_{\alpha=1}^7 \phi_{\nu\nu'}^{(\alpha)}(\underline{z}) w_{\nu'}^{(m,\alpha)}(\underline{z}) \right], \\ \Delta(m - m_\alpha) w_\nu^{(m,\alpha)}(\underline{z}) &= -\frac{2}{r} \sum_{\nu'=0}^{N_\nu} \phi_{\nu\nu'}^{(\alpha)}(\underline{z}) f_{\nu'}^{(m)}(\underline{z}). \end{aligned} \quad (2.12)$$

here  $z = (r, \theta)$  and  $\Delta(m)$  is the 2d Laplacian

$$\Delta(m) \equiv \frac{\partial^2}{\partial r^2} + \frac{1}{r^2} \left[ \frac{\partial^2}{\partial \theta^2} + \frac{1}{\sin \theta} \frac{\partial}{\partial \theta} \sin \theta \frac{\partial}{\partial \theta} - \frac{m^2}{\sin^2 \theta} \right] \quad (2.13)$$

As stated above  $V_{vv'}$  should be derived from the static potential seen by the scattered electron, given by Eq. 2.5. We have shown<sup>6</sup> that the use of an MCSCF  $\Phi_{N_2}$  in (2.14) leads to a slightly less attractive potential than one obtained from an SCF approximation. That result is in qualitative accord with that found by Rumble et al.<sup>8</sup> Very recently, however, Meyer et al.<sup>9</sup> have carefully examined the  $\Pi_g$  resonance in the static exchange approximation and have found that the resonance, using an MCSCF ground state, when the consistent exchange terms are included, corresponds to a slightly more attractive effect than the corresponding consistent exchange approximation with an SCF ground state. Their conclusion (which we find quite surprising, but do not question) is that the use of SCF orbitals for exchange in Eqs. 2.10 and 2.11 is sufficiently inconsistent with the use of an MCSCF wave function in calculating the direct term, that it gives the opposite effect from what is obtained by using the MCSCF wavefunction.<sup>9</sup>

Nevertheless, with regard to our present calculation, we believe this effect is included by the way polarization has been incorporated. To our static potential, we add a polarization potential, as described in Ref. 6:

$$V(\vec{r}; R) \rightarrow V_{static}(\vec{r}; R) + V_{pol}(\vec{r}; R) \quad (2.14)$$

where

$$V_{pol}(\vec{r}; R) = \left(1 - e^{-(r/r_0)^2}\right) V_{pol}^{(OT)}(\vec{r}; R) \quad (2.15)$$

$V_{pol}^{(OT)}$  is calculated from a quasi-ab initio polarized orbital derivation of the polarization potential<sup>4</sup>, but, as seen in (2.15), the latter is diminished in magnitude by a tuning factor,  $(1 - \exp[-(r/r_0)^2])$ , in which  $r_0$  was adjusted to give the  $\Pi_g$  resonance at the correct (i.e. experimental) energy.

We found specifically in Ref. 6 that a value of  $r_0 = 2.430$  was required when using  $V_{static}(MCSCF)$ , whereas  $r_0 = 2.934$  was required for an SCF wavefunction. (There is an unfortunate typographical error in Ref. 6, which read  $r_0 = 2.394$ .) What this implies, in agreement with Meyer et al.<sup>9</sup>, is that although (symbolically)

$$(V_{static} + V_{exch})_{MCSCF} < (V_{static} + V_{exch})_{SCF} < 0, \quad (2.16)$$

because

$$(V_{pol})_{MCSCF} \geq (V_{pol})_{SCF}, \quad (2.17)$$

it is perfectly possible that

$$(V_{static} + V_{exch} + V_{pol})_{MCSCF} \approx (V_{static} + V_{exch} + V_{pol})_{SCF}, \quad (2.18)$$

[To repeat, the above equations culminating in Eq. 2.18 are intended as a measure of “size” in an average sense; in detail, both the  $r$  and  $R$  dependence of each side will be noticeably different from the other. We expect therefore that the left hand side, which derives from the better (MCSCF) wave function, does represent a considerable improvement, and that is what is used here.]

Thus, from the pragmatic point of view of this calculation, we consider the criticism of Ref. 9 to have been overcome; in fact, we believe that the results we shall present are, in the region of the center of the resonance ( $1.6 < k^2 < 3eV$  and  $v \leq 2$ ), the most accurate that have thus far been calculated.

Moreover, the conclusion of Ref. 9 notwithstanding, it is completely possible that if one had included the effect of static polarization, exchange, and correlation simultaneously, (part of such effects would be described by the exchange-polarization terms in a full polarized orbital treatment<sup>10</sup>, for example), and if one had then isolated the piece labelled  $V_{static} + V_{exch}$  separately, then it might have led to the result of Weatherford et al.<sup>6</sup>, that the MCSCF result would be less attractive than the corresponding SCF result [i.e. the reverse of (2.16)].

### III. RESULTS AND COMPARISONS

To the one resonant partial wave ( $\Pi_g$ ), we add the four most important non-resonant partial waves ( $^1\Sigma_g, ^1\Sigma_u, ^1\Pi_u, ^1\Delta_g$ ), calculated in the fixed-plus adiabatic-nuclei approximations, as discussed in Ref. 6. Let us first show and discuss the total cross section  $\sigma_T$  (the sum of all energetically allowed vibrational channels, summed and averaged over rotational states in the usual way). The resonance with its famous substructure<sup>11</sup>, is usually compared, as it is here, with the experimental result of Kennerly.<sup>12</sup> The theoretical curves shown are our previous 10 state result<sup>7</sup> (dashed curve), our present 15 state result (solid curve), compared to experiment and the Schwinger multichannel calculation of Huo et al.<sup>13,14</sup>

With reference to our calculations, the comparison of the 10 and 15 state results gives a good idea of the convergence of the close coupling expansions: we would say that our calculations are well converged to just beyond the first resonance ( $k^2 < 1.95eV$ ), reasonably well converged to just beyond the second ( $\approx 2.2eV$ ), and approximately converged to  $\approx 2.5eV$ . Of particular note, therefore, is the fact that ours is the only calculation which describes the magnitude of the first peak ( $\sigma_T \approx 27\text{\AA}^2$  at  $k^2 = 1.95eV$ ) and gives the ratio of

the first two peaks accurately. The calculation of Huo et al.<sup>14</sup> is almost as satisfactory, while their adjoining paper<sup>13</sup> gives the whole sequence of vibrational excitation cross sections in remarkable accord with experiment.<sup>15</sup>

The ability of such theories as in Refs. 13 and 14 to achieve such an elaborate overview of the entire resonance substructure goes back to the physical ideas underlying the boomerang model (cf. Ref. 17), which have been given their most rigorous justification in the R-matrix theory and calculations of Schneider, LeDourneuf, and VoKyLan.<sup>18</sup> More discussion of these theories will be included in the latter parts of this paper.

In this paper, we shall concentrate on angular distributions. In Fig. 2, we show the elastic differential cross section at 1.50 eV, just below the onset of the  $\Pi_g$  resonance. Also shown are various other theoretical<sup>2,14,19</sup> and experimental<sup>20-22</sup> results. Both similarities and differences are evident. The results continue into the heart of the resonance region ( $k^2 \approx 2.1eV$ ), in Figs. 3 and 4. We have divided those results into two parts: in Fig. 3, we show our present results at three energies surrounding 2.10 eV; one sees how significantly the shape varies over 0.1 eV. This is particularly relevant to the fact that the latest experiment<sup>22</sup> only claims an energy uncertainty of just that amount. Nevertheless, the discrepancy between all these results and the original hybrid theory calculation<sup>2</sup> is clear. In Fig. 4, the same experimental information is compared to the present calculation and that of Huo et al.<sup>14</sup> at 2.10 eV. Here the similarity of the calculated results, both of which provide absolute values, is the most striking feature. It should be noted that an SCF target representation was used in Ref. 14. The agreement between theories suggests that the recent experiment<sup>22</sup> is dominated by the particular energy in the composite beam which gives the dominant cross section at a particular angle.

The comparison of experiment and theory at 3.0 eV is shown in Fig. 5. The similarity of the recently calculated results continues, but — referring back to Fig. 1 — we emphasize that at 3 eV, the energy is definitely pressing the outer edge of reliability of the present calculation. The other interesting feature of the latest experiment<sup>22</sup>, noted there as well, is that the absolute magnitude in the directions  $\theta < 110^\circ$  favors the original hybrid result.<sup>2</sup>

In the next three figures (6,7,8), we show differential cross sections in the excitation transition to the first vibrational state. At the lowest energy (1.50 eV), our present calculation (Fig. 6) is definitely favored by the experiment of Brennan et al.<sup>22</sup>, whereas, in the vicinity of the dominant peak (Fig. 7), that is only true in the middle of the angular range. Note that a different set of experimental results from an Australian group has also been included.<sup>23</sup> At the highest energy, 3 eV, the graph also includes results of an R-matrix calculation<sup>24</sup> and yet another experiment.<sup>25</sup> Here the similarity of the present results with those of the R-matrix calculation is the most notable feature, particularly at middle angles, where they agree best with the experimental results of Ref. 23.

Finally we show in Fig. 9, the angular distribution associated with the excitation of the

second vibrational state in the vicinity of the dominant peak. Here the two experimental results<sup>22,23</sup> are in agreement with each other to within their experimental errors, and they agree best with our present result at the experimental energy 2.10 eV, rather than at its fringes (2.05, 2.15 eV).

#### IV. DISCUSSION

This completes the presentation of the results of this calculation. (More results are available upon request.) Although the method (the hybrid theory) is *ab initio* in principle, it contains here one phenomenological parameter, the polarization cut-off  $r_0$  [cf. Eq. 2.15]. The main practical purpose for doing this is to provide the best cross sections for (several space) applications. It will be recalled that our (hybrid) theory was developed in the context of SAR arcs.<sup>2</sup> The numerical results of that calculation were collected as a NASA document.<sup>26</sup> The present (more accurate) cross sections are intended for the understanding of secondary electron flux in the lower F region of the ionosphere. The specific question concerns whether or not there is a dip in the electron distribution function.<sup>27</sup> Relevant ionospheric calculations are now ongoing at Goddard Space Flight Center<sup>28</sup>, using our cross sections and those of others, principally Huo et al.<sup>13,14</sup>

From a more fundamental point of view, the present results are intended to be a more definitive comparison with experiment in the resonance region, particularly with angular distributions. As we have seen from the comparisons in the previous section, there is still insufficient agreement among experiments themselves to provide a definitive check at this time. In addition, future experiments will require an even finer energy resolution, at a finer energy grid, to be compelling in this regard. This having been said, it is important to acknowledge that great progress in experimental angular distributions, culminating in the recent work of the Australian group<sup>22,23</sup>, has already been made.

With regard to calculational methodology, specifically hybrid vs. R-matrix and/or other  $L^2$  basis set theories, in addition to what was said above and elsewhere<sup>29</sup>, it is clear that the latter are capable of giving the greater overall accuracy at the present time, as is exemplified by the results of Refs. (13,14,18). (In further detail, for example, the R-matrix theory shows that the  $\Pi_g$  resonance is dominated by short range correlations rather than the long range polarizability.) However, if insufficient correlation is included, the R-matrix method and  $L^2$  methods in general, can yield noticeable inaccuracy (cf. Ref. 30, for example).

Furthermore, the basic tenet of the hybrid theory is common to both approaches,<sup>2,29</sup> it is the fact that if the interaction time of the resonance is comparable to vibrational time scales of the target molecule, but short compared to rotation time scales, then in one way

or another, a dynamical treatment of the  $N + 1$  electron system is required. That treatment can be either a dynamical coupling of the incident particle with the vibrational motion of the target, or a recalculation of the Born-Oppenheimer problem of the  $(N + 1)$ -electron system, followed by a calculation of the vibrational spectrum in the (necessarily complex) potential energy well of the compound system.

The drawback of the present methodology is due to the slow convergence of the vibrational close coupling expansion. In principle, that can be overcome by going to a 3d approach in which the internuclear separation ( $R$ ) becomes the third dynamical variable. Such a theory has already been outlined,<sup>31</sup> and the non-iterative pde method<sup>1</sup> has been generalized to three and higher dimensional equations and applied to a solvable model.<sup>32</sup> The implementation of this program is already in progress, however, its completion will not be easy: in particular, the detailed substructure that such calculations reveal, will depend critically on the range and mesh size with which the  $R$  variable can be covered.

Perhaps the most exciting potential application of the 3d pde technique, also discussed in Ref. 32, is the fact that it can be applied to scattering (in principle) from arbitrary polyatomics in the fixed-nuclei approximation.<sup>33</sup> Augmented by the adiabatic-nuclei approximation,<sup>33</sup> such a method would be an invaluable tool in studying scattering processes in galactic environments, such as the Orion nebula, where it is known that exotic molecules can form (cf. Ref. 34, for example) which may not be amenable to laboratory experimentation, so that theoretical calculation provides the only reasonable alternative.

## ACKNOWLEDGEMENTS

Work of A.T. was done under NASA RTOP 432-36-58-01. C.A.W. was partially supported by NASA grant NAG-5307, NCC 2-492 and NASA contract NAGW-2930; he would also like to acknowledge a grant of computer time by Florida State University on a CRAY-YMP.

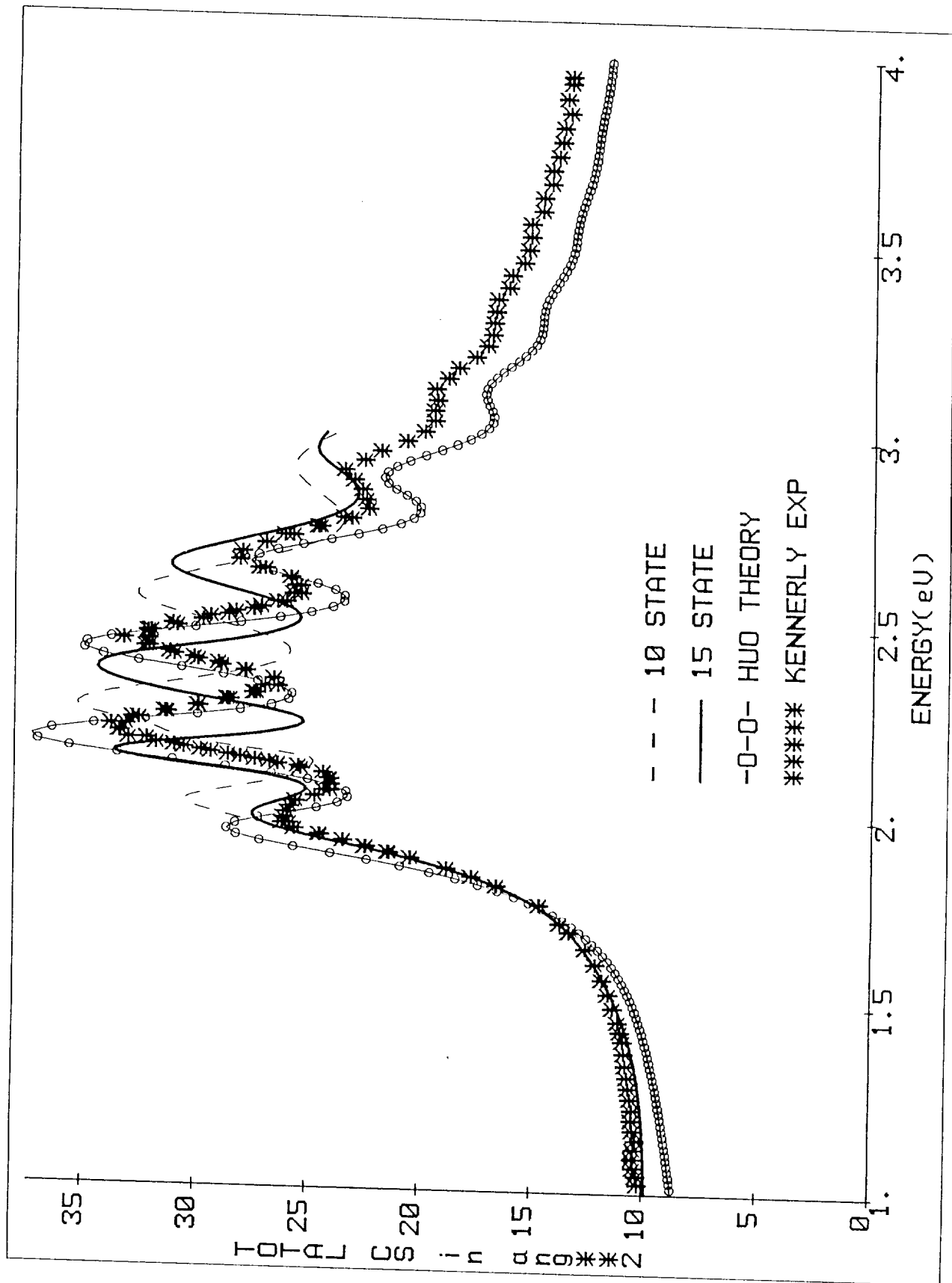
## REFERENCES

1. E.C. Sullivan and A. Temkin, *Comp. Phys. Comm.* **25**, 97 (1982).
2. N. Chandra and A. Temkin, *Phys. Rev.* **A13**, 188 (1976).
3. A. Temkin in *Symposium on Electron – Molecule Collisions*, ed. by I. Shimamura and M. Matsuzawa.
4. K. Onda and A. Temkin, *Phys. Rev.* **A28**, 621 (1983).
5. C.A. Weatherford, K. Onda, and A. Temkin, *Phys. Rev.* **A31**, 3620 (1985).

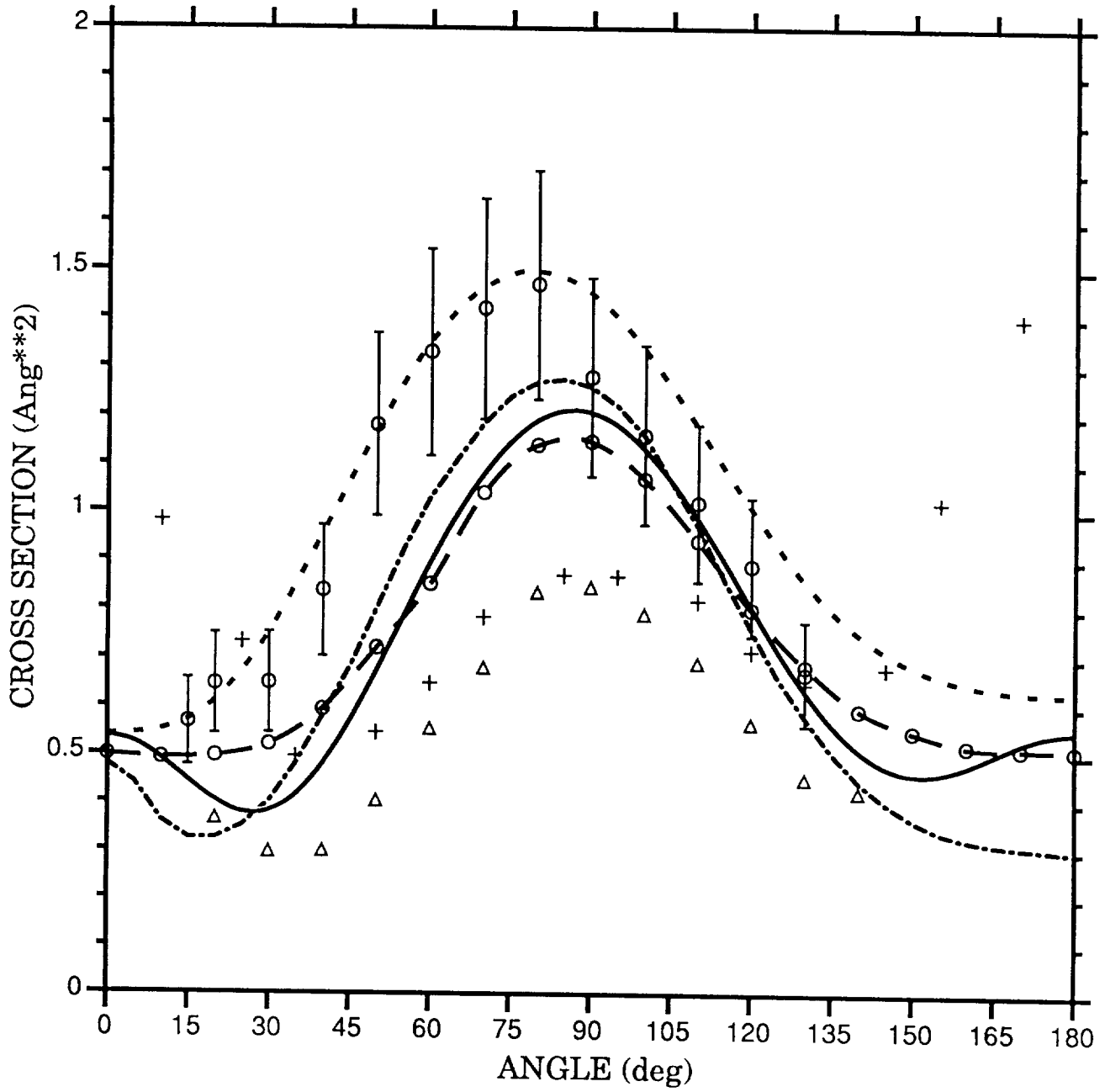
7. C.A. Weatherford and A. Temkin in *Electron – Molecule Scattering and Photoionization*, ed. by P.G. Burke and J.B. West (Plenum Press, N.Y. and London, 1988), p. 229.
8. J.R. Rumble, W. J. Stevens, and D.G. Truhlar, *J. Phys.* B17, 3151 (1984).
9. H.-D. Meyer, S. Pal, and U. Riss, *Phys. Rev.* A46, 186 (1992).
10. A. Temkin, *Phys. Rev.* 107, 1004 (1957).
11. D.E. Golden, *Phys. Rev. Lett.* 17, 847 (1966).
12. R.E. Kennerly, *Phys. Rev.* A21, 1876 (1980).
13. W.H. Huo, T.L. Gibson, M.A.P. Lima, and V. McKoy, *Phys. Rev.* A36, 1632 (1987).
14. W.H. Huo, M.A.P. Lima, T.L. Gibson, and V. McKoy, *Phys. Rev.* A36, 1642 (1987).
15. M. Allan, *J. Phys.* B18, 4511 (1985).
16. L.A. Morgan, *J. Phys.* B19 L439 (1986).
17. L. Dube and A. Herzenberg, *Phys. Rev.* A20, 194 (1979).
18. B.I. Schneider, M. LeDourneuf, and VoKyLan, *Phys. Rev. Lett.* 43, 1926 (1979).
19. M.A. Morrison, B.C. Saha, T.L. Gibson, *Phys. Rev.* A76 3682 (1987).
20. T.W. Shyn and G.R. Carignan, *Phys. Rev.* A22, 923 (1980).
21. W. Sohn, K.-H. Kochem, K.-M. Scheuerlein, K. Jung, H. Ehrhardt, *J. Phys.* B19, 5017 (1986).
22. M.J. Brennan, D.J. Alle, P. Euripides, S. Buckman, and S.J. Brunger, *J. Phys.* B25, 2669 (1992).
23. M.J. Brunger, P.J.O. Teubner, A.M. Wiegold, and S.J. Buckman, *J. Phys.* B22, 1443 (1989).
24. C.J. Gillan, O. Nagy, P.G. Burke, L.A. Morgan, and C.J. Noble, *J. Phys.* B20, 4585 (1987).
25. H. Tanaka, T. Yamamoto, and T. Okada, *J. Phys.* B14, 2081 (1981).
26. N. Chandra and A. Temkin, NASA Technical Note TN D-8347, 1976.
27. P.G. Richards, D.G. Torr, and W.A. Abdou, *J. Geophys. Res.* 91, 304 (1986).
28. W.R. Hoegy (work in progress; we thank Dr. Hoegy for valuable discussions on the space physics aspects of this problem).
29. A. Temkin in *Electronic and Atomic Collisions*, ed. by N. Oda and K. Takayanagi, (North Holland Publ. Co., 1980) p. 95.
30. L.A. Morgan, *J. Phys.* B19, L439 (1986).
31. A. Temkin, C.A. Weatherford, and E.C. Sullivan, AIP Conf. Proc. 204, A. Herzenberg ed. (AIP, N.Y., 1990), p. 133.
32. E.C. Sullivan and A. Temkin, *Comp. Phys. Comm.* 71, 319 (1992).
33. A. Temkin, K.V. Vasavada, E.S. Chang, and A. Silver, *Phys. Rev.* 182, 57 (1969).
34. *Molecules in the Galactic Environment*, M.A. Gordon and L.E. Snyder eds. (John Wiley & Sons, N.Y., 1973).

## Figure Captions

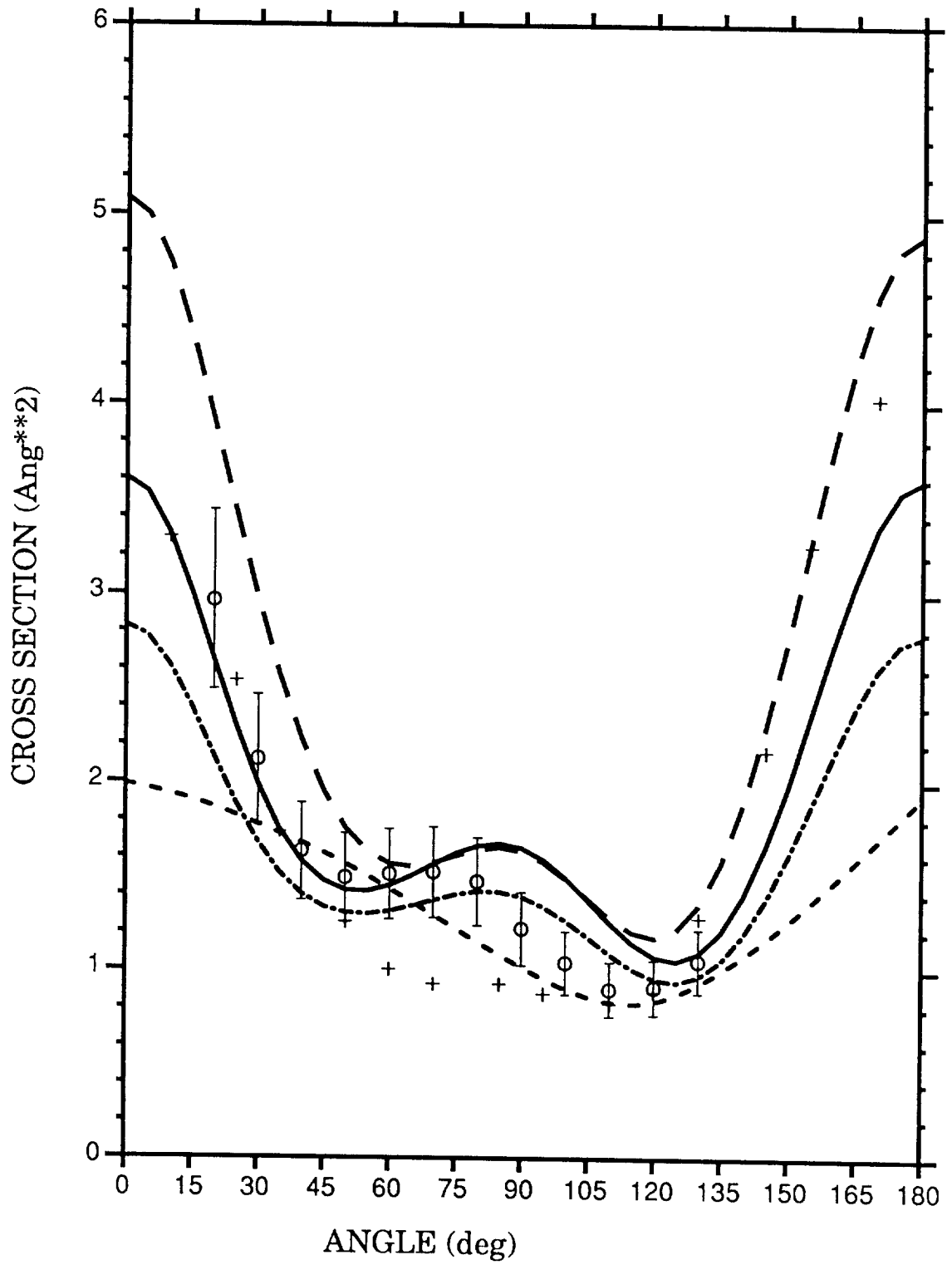
- Fig. 1. Total integrated cross section in square Angstroms ( $\text{A}^2$ ): Experiment: (\*\*\*) Ref. 12. Theory: (—) present [15 state results]; (- - -) our 10 state results (Ref. 7); (-o-o-o-) Ref. 14.
- Fig. 2.  $d\sigma_{00}/d\Omega$  at 1.50 eV: Theory: (—) present; (-o-o-o-) Ref. 14; (- - -) Ref. 2; (— — —) Ref. 19. Experiment: ( $\Phi\Phi\Phi$ ) Ref. 22; (+++) Ref. 20; ( $\Delta\Delta\Delta$ ) Ref. 21.
- Fig. 3.  $d\sigma_{00}/d\Omega$ . Theory: (— — —) present at 2.05 eV; (—) present at 2.10 eV; (— — —) present at 2.15 eV; (- - -) Ref. 2. Experiment: ( $\Phi\Phi\Phi$ ) Ref. 22; (+++) Ref. 20.
- Fig. 4.  $d\sigma_{00}/d\Omega$  at 2.10 eV. Theory: (—) present; (-o-o-o-) Ref. 14. Experiment: ( $\Phi\Phi\Phi$ ) Ref. 22; (+++) Ref. 20.
- Fig. 5.  $d\sigma_{00}/d\Omega$  at 3.00 eV. Theory: (—) present; (- - -) Ref. 2. Experiment: ( $\Phi\Phi\Phi$ ) Ref. 22; (+++) Ref. 20.
- Fig. 6.  $d\sigma_{01}/d\Omega$  at 1.50 eV. Theory: (—) present; (- - -) Ref. 2. Experiment: ( $\Phi\Phi\Phi$ ) Ref. 22; ( $\Delta\Delta\Delta$ ) Ref. 21.
- Fig. 7.  $d\sigma_{01}/d\Omega$ : Theory: (— — —) present at 2.05 eV; (—) present at 2.10 eV; (— — —) present at 2.15 eV; (- - -) Ref. 2. Experiment: ( $\Phi\Phi\Phi$ ) Ref. 22; ( $\infty\infty$ ) Ref. 23.
- Fig. 8.  $d\sigma_{01}/d\Omega$  at 3.00 eV. Theory: (—) present; (- - -) Ref. 2; (— — —) Ref. 24. Experiment: ( $\Phi\Phi\Phi$ ) Ref. 22; ( $\infty\infty$ ) Ref. 23; ( $\bullet\bullet\bullet$ ) Ref. 25.
- Fig. 9.  $d\sigma_{02}/d\Omega$ : Theory: (— — —) present at 2.05 eV; (—) present at 2.10 eV; (— — —) present at 2.15 eV; (- - -) Ref. 2. Experiment: ( $\Phi\Phi\Phi$ ) Ref. 22; ( $\infty\infty$ ) Ref. 23.



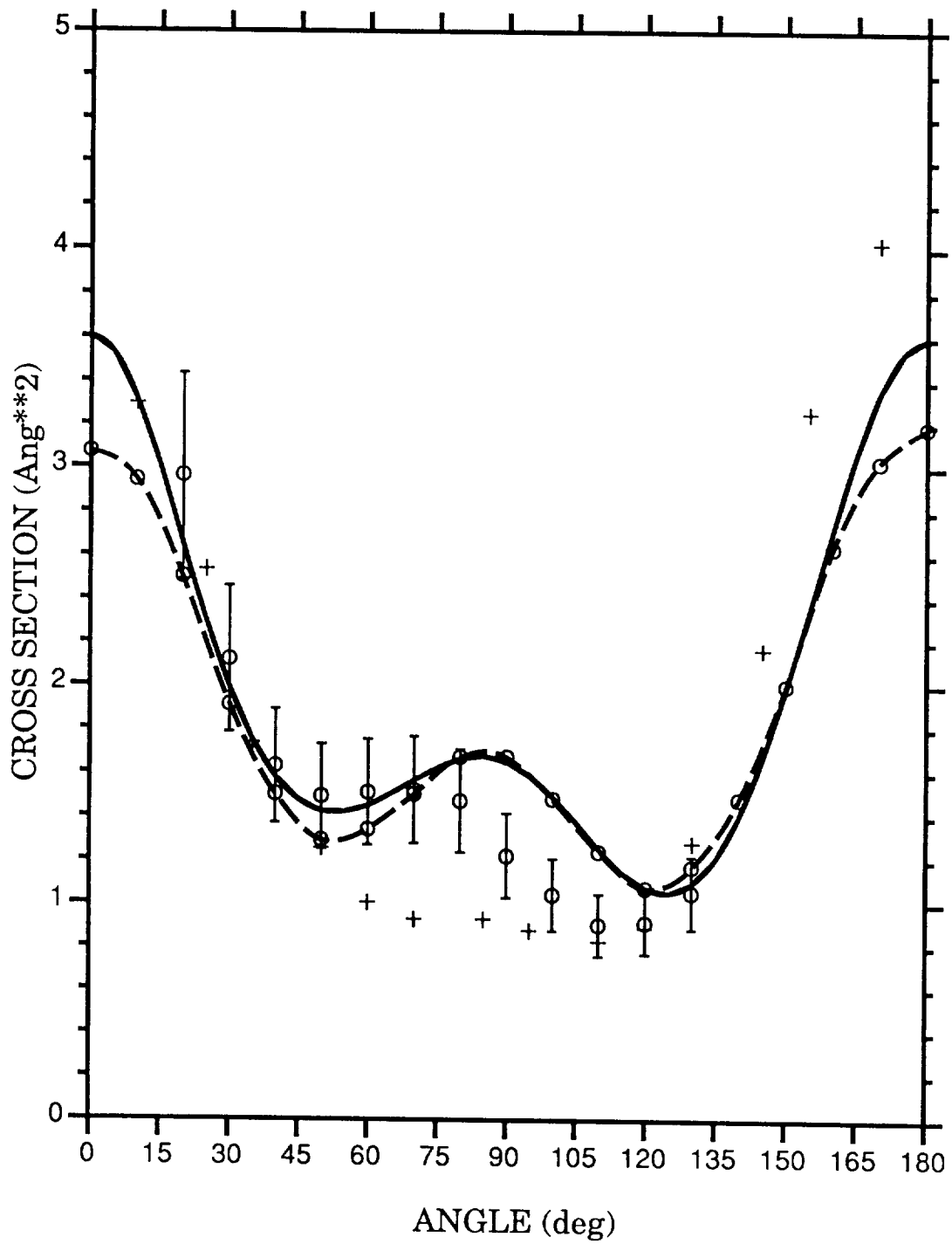
$e^- + N_2 : v(0 \rightarrow 0)$   
DIFFERENTIAL C/S  
1.50 eV



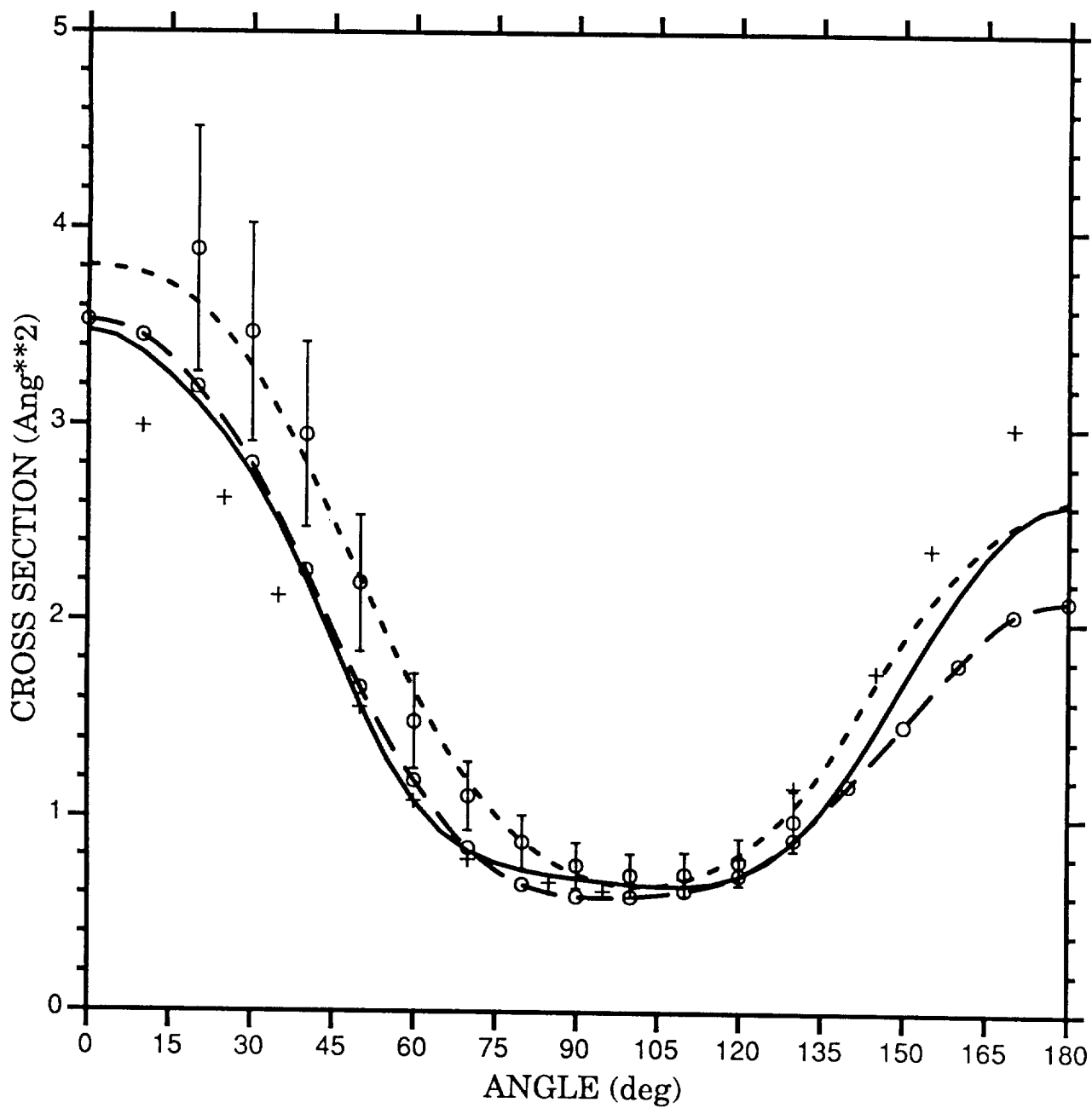
$e^- + N_2 : v(0 \rightarrow 0)$   
DIFFERENTIAL C/S  
2.05, 2.10, 2.15 eV



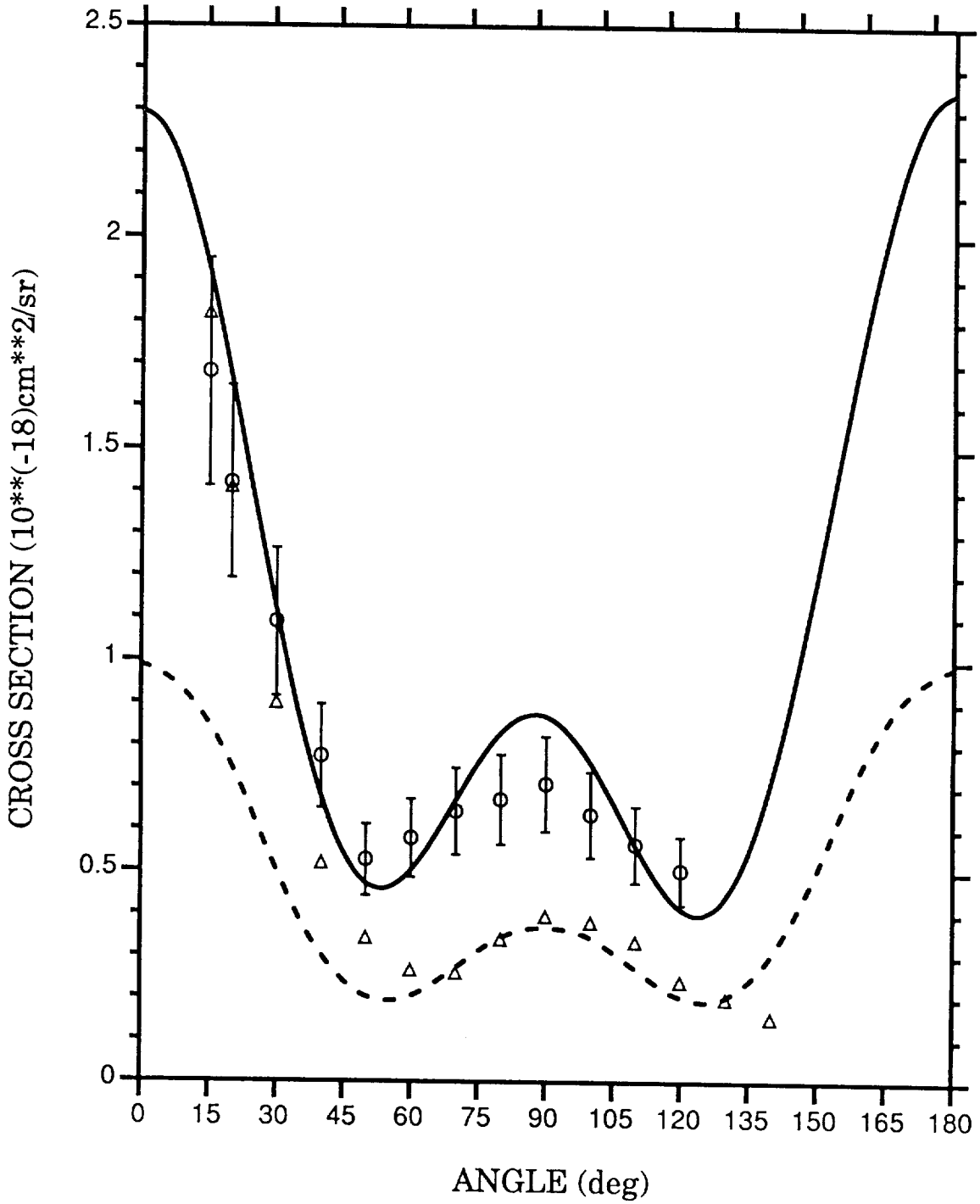
$e^- + N_2: v(0 \rightarrow 0)$   
DIFFERENTIAL C/S  
2.10 eV



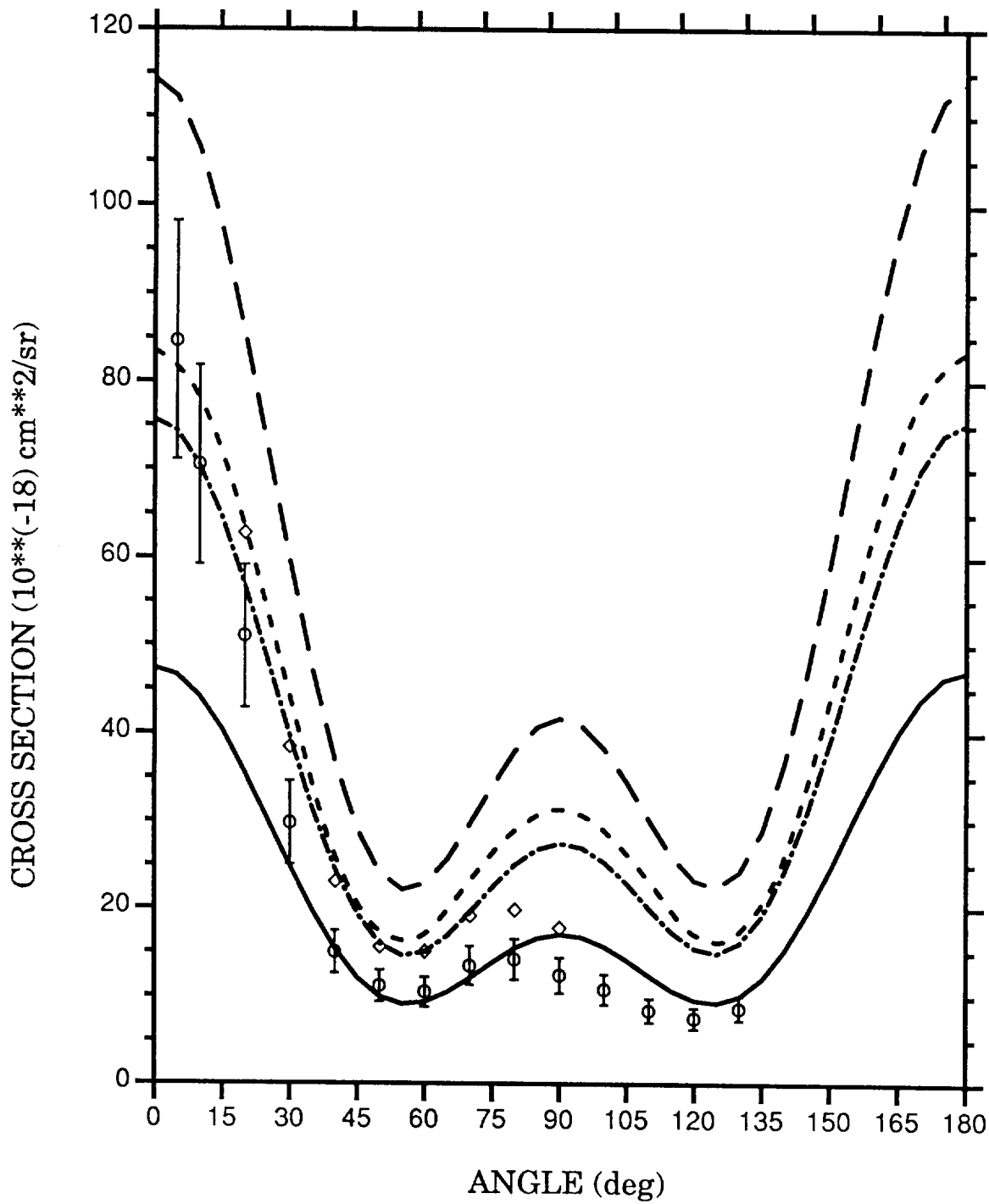
$e^- + N_2 : v(0 \rightarrow 0)$   
DIFFERENTIAL C/S  
3.00 eV



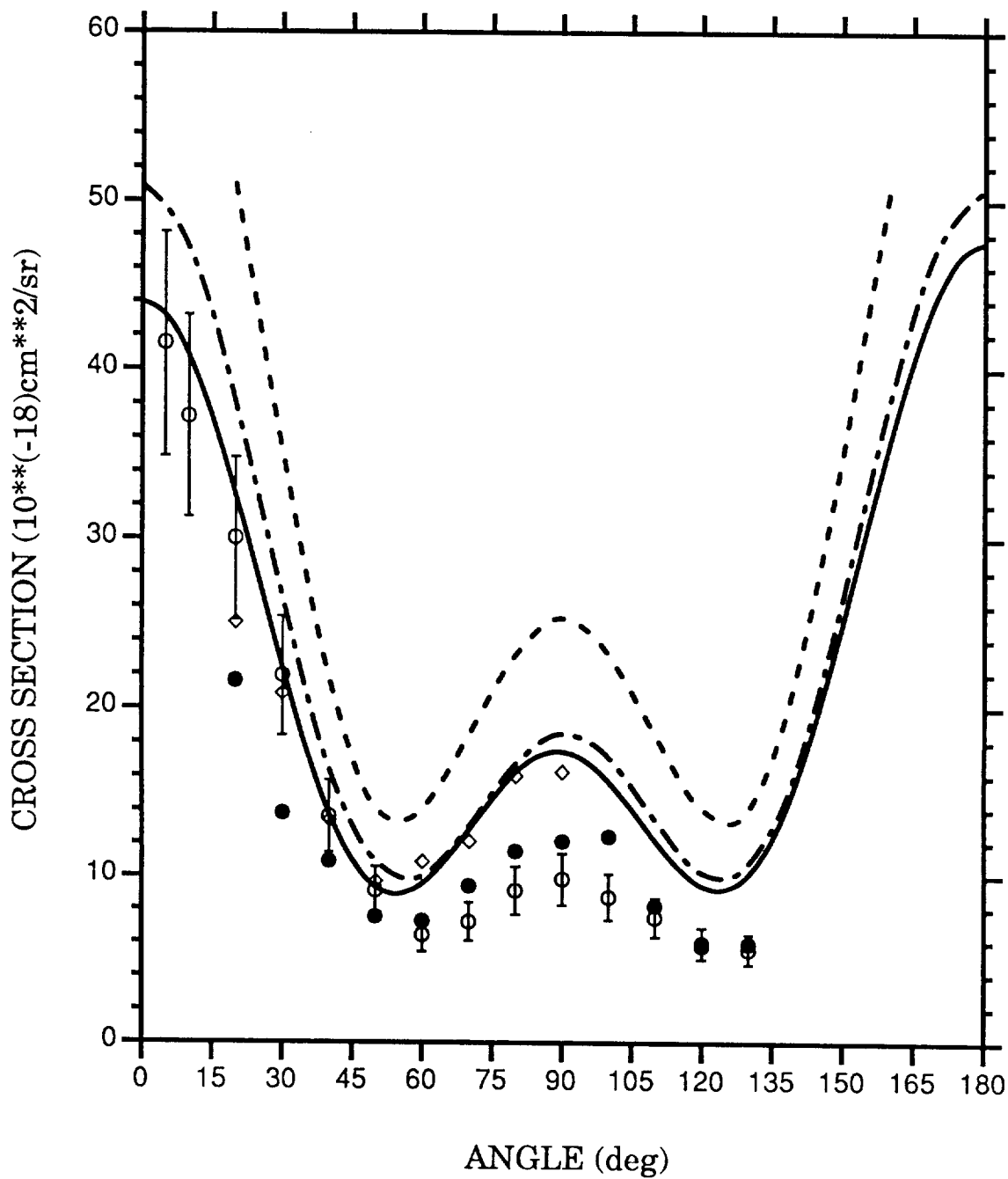
$e^- + N_2 : v(0 \rightarrow 1)$   
DIFFERENTIAL C/S  
1.50 eV



$e^- + N_2 : v(0 \rightarrow 1)$   
DIFFERENTIAL C/S  
2.05, 2.10, 2.15 eV



$e^- + N_2 : v(0 \rightarrow 1)$   
DIFFERENTIAL C/S  
3.00 eV



$e^- + N_2 : v(0 \rightarrow 2)$   
DIFFERENTIAL C/S  
2.05, 2.10, 2.15 eV

